ACS OMEGA

Open Access

http://pubs.acs.org/journal/acsodf

Article

Synthesis of "Ice Cube" Shaped Zeolite A Type and Cu^{2+} Ion-Exchanged Zeolites and Study of Their CO_2 Adsorption Performance

Jayaprakash Madhu,* Agilan Santhanam, and Dhayalan Velauthapillai

Cite This: *ACS Omega* 2024, 9, 45926−45942

Read Online

ACCESS | Metrics & More | Article Recommendations | Supporting Information

ABSTRACT: In this study, zeolite type A and four Cu^{2+} ion-exchanged zeolites were synthesized through cationic ion exchange process with Cu concentrations of 0.05, 0.1, 0.15, and 0.2 M respectively. The physicochemical properties of both the prepared and ion-exchanged zeolites were thoroughly analyzed. Field Emission Scanning Electron Microscopy (FESEM) micrographs revealed that the synthesized zeolites exhibited an "ice cube"-shaped morphology, and this morphology was maintained even after the ion exchange process. N_2 adsorption/desorption studies indicated a typical type IV isotherm with an H3 hysteresis loop for both the prepared and Cu^{2+} ion-exchanged zeolites. CO_2 adsorption data followed a type I isotherm, with the highest adsorption capacity of 4.02 mmol/g observed for the 0.1 M Cu^{2+} ion-exchanged zeolites. The adsorption behavior was modeled using a nonlinear isotherm, with good agreement between experimental and fitted data.

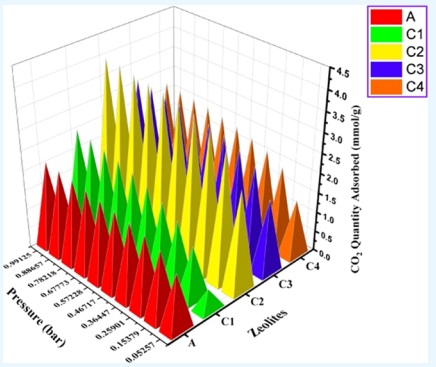

1. INTRODUCTION

One of the primary reasons for the greenhouse effect's escalation is the burning of fossil fuels, which releases carbon dioxide into the atmosphere. Due to the excessive energy demand in the industrial sectors, there is a rapid increase in pollution, which results in the enormous release of CO_2 into the atmosphere.[1] On the other hand, increased awareness of climate change has prompted the usage of technology to reduce greenhouse gas emissions. Despite the accessibility of renewable and other alternative energy supplies, fossil fuels remain as the world's principal energy source, and finding a viable replacement for them is a challenging task.[2] Many environmental problems have arisen as a result of the significant increase in CO_2 emissions, which has increased from 280 to 410 ppm between 1760 and 2020. The average world temperature has risen by 1 °C as a consequence of the significant emission of greenhouse gases.[3,4] According to the International Energy Agency (IEA) publication's Energy Perspective 2020, carbon capture and storage are going to be critical in implementing the Paris Agreement. Consequently, steps are being taken to stop major climate change by bringing the global temperature down by 2 °C.[4,5]

For the CO_2 capture process techniques such as membrane separation, adsorption, absorption, and cryogenic distillation are most often used to reduce the CO_2 release concentration internationally. Flue gas CO_2 separation is traditionally accomplished by using an alkanolamine-based absorption technique. Even though the method performs better, it still needs to be modified extensively to prevent corrosion and the energy penalty because of oxygen present in the flue gases. However, it appears that the "perfect" sorbents that meet every need are still unattainable.[6] For instance, solid adsorbents have drawn a lot of interest due to their exceptional selectivity and CO_2 adsorption capacity, they have been found to be viable substitutes for amine-based aqueous CO_2 capture methods.[7] Additionally, the adsorption process is easily accessible for several adsorption regenerative processes that use relatively less energy and produce less corrosion. The effective solid adsorbents for CO_2 capture should be inexpensive, show selective adsorption for CO_2, have a large pore volume and high surface area, and allow quick intraparticle diffusion.[7,8]

There are several porous solid adsorbents that can be used to accomplish the gas adsorption process. Solid adsorbents, such as a metal−organic framework (MOF), are well recognized for their large surface area and changeable pore surface. Because of their superior adsorption selectivity, they perform as good CO_2 adsorbents. However, compared to that of other adsorbents, their adsorption is still limited. Their industrial applications are further limited due to their low availability, high cost, and poor chemical and thermal stability. On the other hand, zeolitic imidazolate framework (ZIF) has been widely employed in CO_2 adsorption because of its high performance and diversity of structures.[9] However, there are substantial drawbacks with ZIF such as high-cost material synthesis and inadequate chemical and thermal durability. Activated carbon (AC) has a high surface

Received: June 12, 2024
Revised: October 11, 2024
Accepted: October 16, 2024
Published: November 7, 2024

area compared to the other materials which is favorable for CO_2 adsorption. However, it has drawbacks of its own, such as low thermal durability at higher temperatures, which limits the amount of CO_2 that can be adsorbed.[10] Several researchers are currently working to find solutions for the problems mentioned by utilizing materials that are economically feasible and have high adsorption and improved CO_2 selectivity.

In recent years, zeolite, the porous solid adsorbent, has been considered a promising material for CO_2 adsorption because of its better framework constructive structure. Zeolites are widely recognized for having excellent ion exchange capabilities, great heat and chemical durability, and they benefit from the variable Si/Al ratio, which makes them ideal for high CO_2 adsorption properties.[11] In general, zeolites are hydrated aluminosilicates that contain alkali or alkaline earth metal cations linked through oxygen atoms to a 3-dimensional tetrahedral TO_4 (T = Si or Al). The tetrahedral atoms joined by oxygen create the primary building block unit (PBU). Repeated PBUs combine to form secondary building units (SBU), which lead to the 3-dimensional zeolite framework structure. Zeolites are naturally occurring materials, however in recent years, synthetic materials have received much attention since they can be readily altered in size and shape according to specific requirements. The application of zeolites in industrial technology has grown during the 20th century. The commercial world has witnessed the rise of new synthetic zeolite materials due to the development of novel architectures by researchers inspired by the growing interest in microporous materials.[12]

In recent years, ion-exchange zeolites have caught great attention due to their properties that are suitable for many applications. The adsorption capability of zeolites is greatly influenced by the state, number, and arrangement of cations within the framework.[7,13] Microporous solids have drawn a lot of attention due to their capacity to interact with species both on the outside and within their internal porous network. The presence of cations balances the negative charge inside the porous zeolite framework porous structure. This makes zeolites exhibit ion-exchange properties, which enables the zeolite to incorporate various metal ions for catalytic applications. The most common cationic ion exchange materials are lithium (Li), potassium (K), lead (Pb), copper (Cu), zinc (Zn), ammonia (NH_3), and silver (Ag). Through an ion exchange procedure, transition metals can be added to the zeolite structure to improve its performance, and open up for potential applications.[14]

Tao et al.[15] in their recent research, have reported about the adsorption of CO_2, N_2, and CH_4 by metal cation-exchanged LTA zeolites (Si/Al = 3 and 6) in the 0.04−100 kPa pressure range. Na^+, Ca^{2+}, Mn^{2+}, and Ce^{3+} were chosen as representative examples of monovalent alkali metal cations, divalent alkaline earth metal cations, divalent transition metal cations, and trivalent transition metal cations, respectively. The benchmark used in this study is proton (H^+) from LTA zeolites. In their study, they confirmed that, at moderate pressures, metal cation-exchanged small-pore zeolites are efficient adsorbents for capturing carbon. Wang et al.[16] have synthesized zeolite X from agricultural waste rice hull ash (RHA). Rare earth metal cations such as lanthanum (La) and cerium (Ce) of about 0.2 M were used as ion exchange cations in their work. They also studied the physical properties of the materials by using CO_2 adsorption/desorption experiments.

Liu et al.[17] synthesized Zeolite NaKA with varying proportions of Na^+ and K^+ cations through an ion-exchange method. The proportion of potassium to the total cations K^+/(Na^+ + K^+) was varied from (0 to 97.0 atom %) by adjusting the concentration of potassium chloride, as well as the temperature and duration of the ion exchange process. Their research demonstrated that optimizing the potassium content enhances the selective adsorption of CO_2 over N_2. They concluded that lower ion exchange concentrations have a more significant impact on CO_2 adsorption than intermediate or higher concentrations. Wang et al.[18] in their study utilized rice husk ash as a raw material to prepare Na-ZSM-5 zeolite through a hydrothermal method. This zeolite was then modified through cation exchange using various cations such as Li^+, Mg^{2+}, Ca^{2+}, Cu^{2+}, Zn^{2+}, La^{3+}, and Ce^{3+}. The process was achieved via solution impregnation by adjusting the molar ratio to about (0.2−0.3 M), respectively. They also found that ZSM-5 zeolites modified with transition metal cations Cu^{2+} and Zn^{2+} exhibit the highest adsorption capacities at 0 °C, with values of 70.24 and 74.38 cm^3/g, respectively.

Based on the reviewed literature, it has been identified that lower concentrations of ion exchange are preferable for enhancing the CO_2 adsorption efficiency. This insight guided the optimization of our process, where a lower concentration (0.05, 0.1, 0.15, and 0.2 M) was chosen to achieve high CO_2 adsorption performance. Also, higher concentration may lead to changes in the preferred framework structure.

Furthermore, to the best of our knowledge, only a few reported efforts have been made to synthesize copper ion-exchanged zeolite A type materials, highlighting their superior CO_2 adsorption properties. In this view, the present work focuses on the synthesis of zeolite NaA material using the hydrothermal method. Another primary goal of this work is to optimize the cationic ion exchange method for synthesizing copper ion-exchanged zeolites. They were synthesized through a cationic ion exchange process using copper concentrations of 0.05, 0.1, 0.15, and 0.2 M respectively. Initially, insights into the chemical and textural properties of the prepared and copper ion-exchanged zeolites were studied through a combination of characterization techniques. Then their CO_2 adsorption/desorption performance is measured at an operating temperature of 297.15 K and is discussed in detail. Moreover, we also studied the fitted adsorption isotherm of Langmuir, Freundlich, and Toth adsorption isotherms with experimentally observed CO_2 adsorption data.

2. EXPERIMENTAL SECTION

2.1. Preparation of Zeolite NaA. The synthesis procedure outlines the preparation of zeolite NaA, denoted as "A", using a hydrothermal method. Zeolite NaA with a molar ratio of 2 Na_2O: Al_2O_3:1.96 SiO_2:132 H_2O was synthesized by using the hydrothermal method without using any organic templating agent. Typically, two identical solutions were prepared separately, each containing 40 mL of double distilled (DD) water and 0.295 g of sodium hydroxide (NaOH). These solutions were designated as SOL A and SOL B. Then, 2.46 g of sodium aluminate ($NaAlO_2$) was added to SOL A, while 3.31 g of sodium silicate (Na_2SiO_3), was added to SOL B. Both solutions are stirred for 30 min at room temperature to ensure homogeneity. SOL B is then added quickly to SOL A, and the mixture is stirred for an additional 30 min at room temperature until homogeneity is achieved. The resulting hydrogel, formed from the mixture, is transferred to a Teflon-lined stainless-steel autoclave and subjected to hydrothermal crystallization. The autoclave is maintained at 100 °C for 12 h in a thermostat-

https://doi.org/10.1021/acsomega.4c05487
ACS Omega 2024, 9, 45926−45942

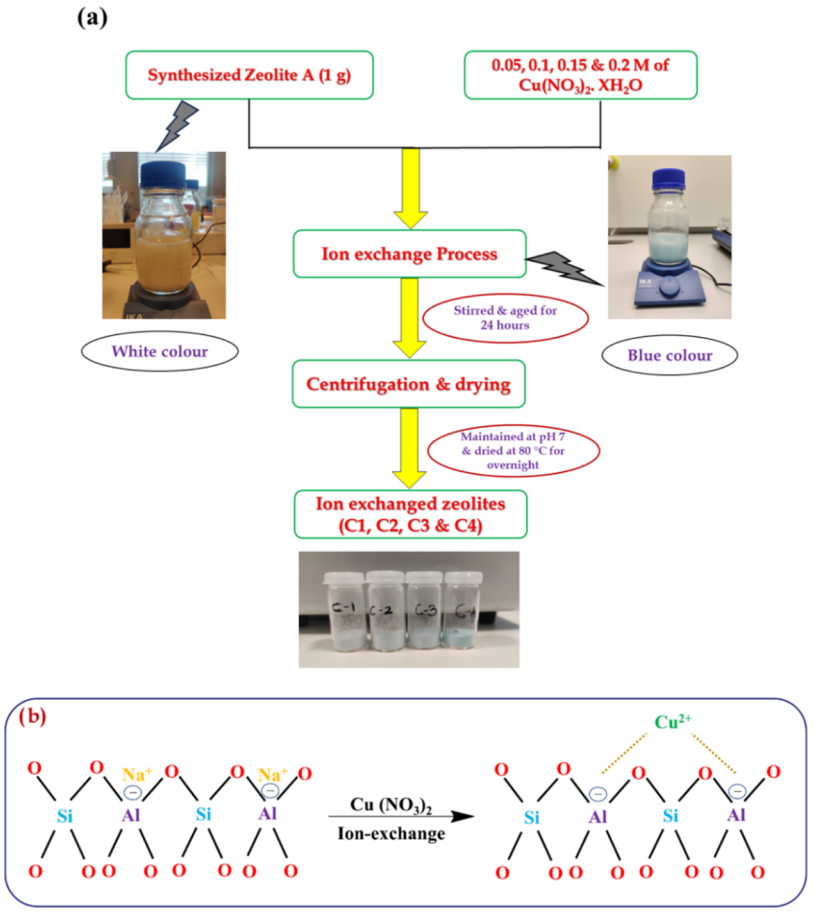

Figure 1. (a) Schematic representation of the synthesis of ion-exchanged zeolites and (b) Illustrating the synthesis scheme of Cu^{2+} ion-exchange zeolites.

controlled oven to facilitate the crystallization process. After crystallization, the hydrogel is washed repeatedly with DD water to reduce the pH to 7. The washing process is carried out to remove unreacted silica and alumina source materials along with sodium cations if any are present in them. The obtained crystalline residue products from the centrifugation step are then desiccated at 80 °C overnight in an oven to remove any remaining moisture and to obtain the final zeolite NaA product.

The following equation, representing the possible synthesis mechanism of zeolite NaA-type materials, has been derived from existing literature and validated in accordance with established methodologies and findings, ensuring consistency with previous reported data.[19,20]

$$\mathrm{NaOH(aq) + NaAl(OH)_4(aq) + Na_2SiO_3(aq)} \xrightarrow{T1\approx 25^{\circ}\mathrm{C\ (Room\ Temperature)}} [\mathrm{Na_a(AlO_2)_b(SiO_2)_c \cdot NaOH \cdot H_2O}]\ \text{(amorphous gel)} \quad (1)$$

$$[\mathrm{Na_a(AlO_2)_b(SiO_2)_c \cdot NaOH \cdot H_2O}] \xrightarrow{100^{\circ}\mathrm{C\ for\ 12\ h}} \mathrm{Na_x[(AlO_2)_x(SiO_2)_y] \cdot mH_2O} + \text{solution}\ [\text{zeolite NaA}] \quad (2)$$

Equation 1 illustrates the formation of an amorphous gel when NaOH, $NaAl(OH)_4$, and Na_2SiO_3 react together at room temperature. This gel formation results mainly from the copolymerization of silicate and aluminate species during the condensation-polymerization process. Equation 2 shows that maintaining the hydrothermal condition for 12 h at 100 °C leads to the transformation of the amorphous gel into a crystalline phase of zeolite NaA-type material.[19,21]

2.2. Preparation of Zeolite Cu^{2+} Ion Exchange Process.

To prepare Cu^{2+} ion-exchanged zeolites, copper nitrate was employed as the source material for the ion-exchange process. For the synthesis of CuA zeolites, the cation exchange process was carried out. 0.05 M Cu^{2+} ion-exchanged zeolite was synthesized by using copper nitrate as the cation exchange source material. Copper nitrate is dissolved in DD water to prepare a solution with a desired concentration. The amount of copper nitrate used determines the concentration of Cu^{2+} ions in the solution. Then 1 g of synthesized zeolite is added to the copper nitrate solution. The mixture is aged and stirred for 24 h to facilitate the ion exchange process, during which Cu^{2+} ions from the solution replace some of the original cations in the zeolite structure. The ion-exchanged products are recovered by centrifugation to separate them from the solution. The recovered products are dried in an oven at 80 °C overnight to remove any remaining moisture and the obtained product is named C1. Similarly, for 0.1, 0.15, and 0.2 M copper ion exchanged zeolites, an appropriate amount of copper nitrate was added separately to 100 mL of DD water. For each 100 mL of copper nitrate solution, 1 g of zeolite was added, and then the solution was aged and stirred for 24 h to ensure the uniform distribution of ions throughout the solution. Finally, the ion-exchanged products were obtained through centrifugation and

https://doi.org/10.1021/acsomega.4c05487
ACS Omega 2024, 9, 45926−45942

then dried in an oven at 80 °C overnight. The obtained ion-exchanged products are named C2, C3, and C4, representing different concentrations of Cu^{2+} ions in the zeolites.

The schematic representation of the ion exchange process is depicted in Figure 1a, illustrating the sequence of steps involved in the process. The scheme for the formation of ion exchange Cu^{2+} zeolites is shown in Figure 1b.[22] The mechanism, denotes the reaction between two monovalent sodium (Na^{+}) cations were replaced by one divalent copper (Cu^{2+}) cation to form the respective copper ion-exchanged zeolites.[22,23]

3. RESULTS AND DISCUSSION

3.1. X-ray Diffraction (XRD) Studies. The powder X-ray diffractogram is used to analyze the type and purity of the prepared and ion-exchanged zeolite materials. Figure 2a–e displays the diffraction patterns of both the prepared and ion-exchanged zeolites, with patterns observed within the 2θ range of 5–50°. The presence of sharp peaks in these patterns indicates the crystalline nature of the materials. The indexed peaks closely match with the previously reported data.[24,25]

The XRD patterns of the prepared and ion-exchanged zeolites are shown in Figure 2a–e. The recorded diffraction patterns

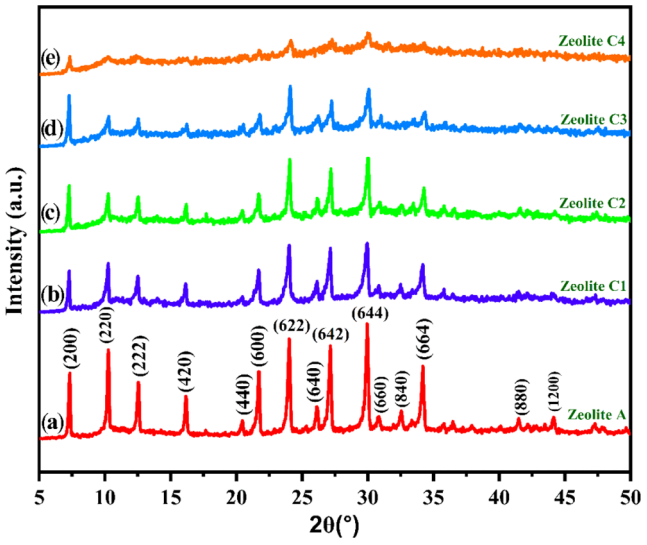

Figure 2. X-ray diffraction pattern of (a) prepared zeolite A type and (b–e) Cu^{2+} ion-exchanged zeolites (C1–C4).

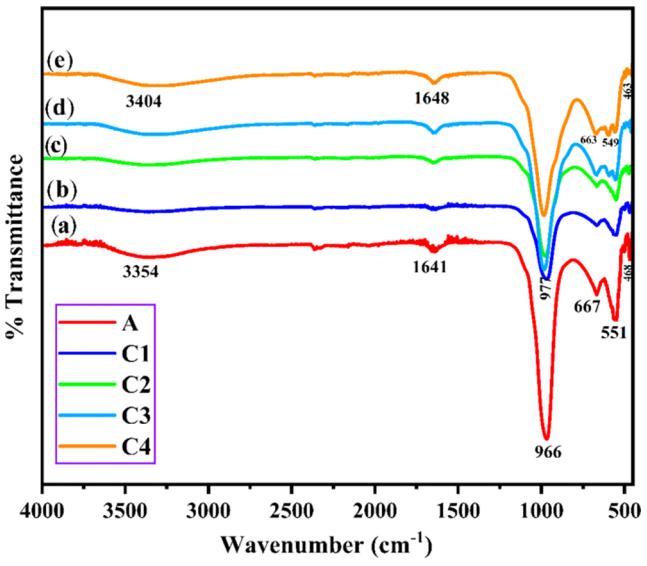

Figure 3. Fourier Transform Infrared spectra of (a) prepared zeolite A type and (b–e) Cu^{2+} ion-exchanged zeolites (C1–C4).

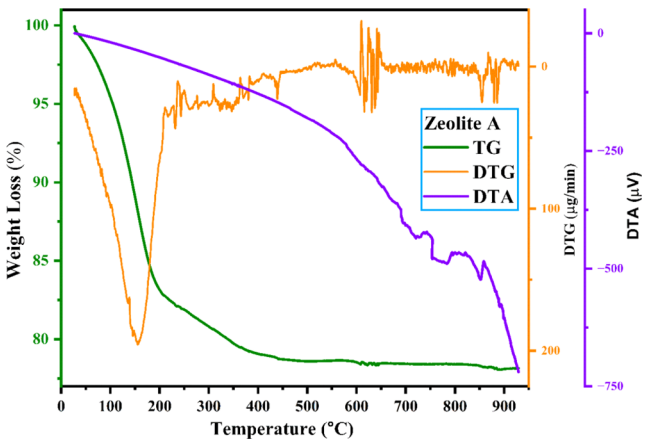

Figure 4. Thermogravimetric/Differential thermal analysis (TG/DTA) analysis of the prepared zeolite A type.

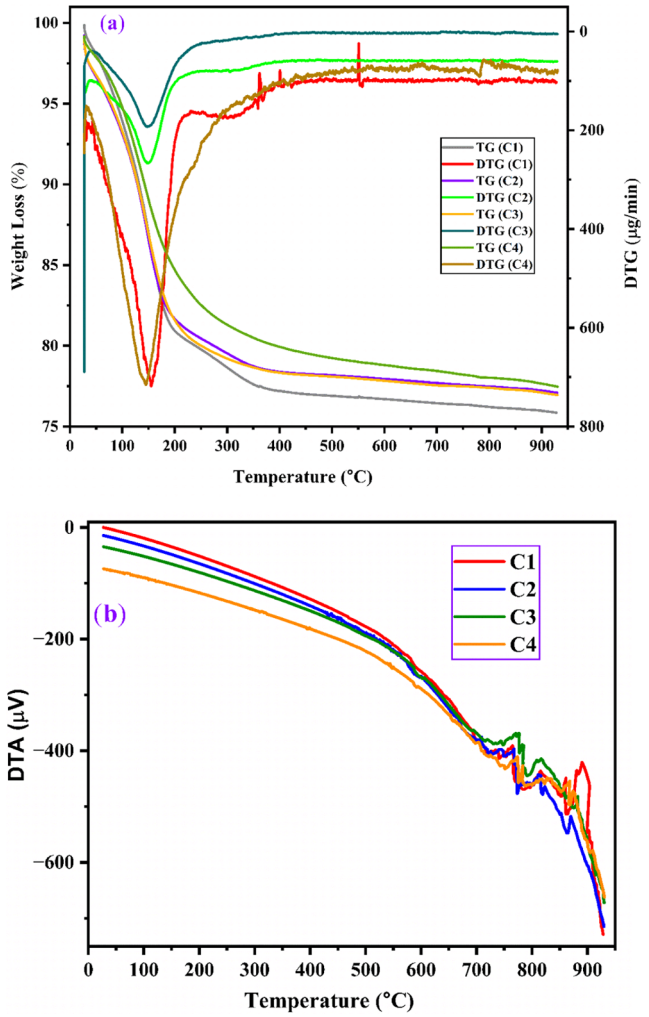

Figure 5. (a) Thermogravimetric and derivative thermogravimetric analysis (TG/DTG) and (b) Differential thermal analysis (DTA) analysis of the Cu^{2+} ion-exchanged zeolites (C1–C4).

https://doi.org/10.1021/acsomega.4c05487
ACS Omega 2024, 9, 45926–45942

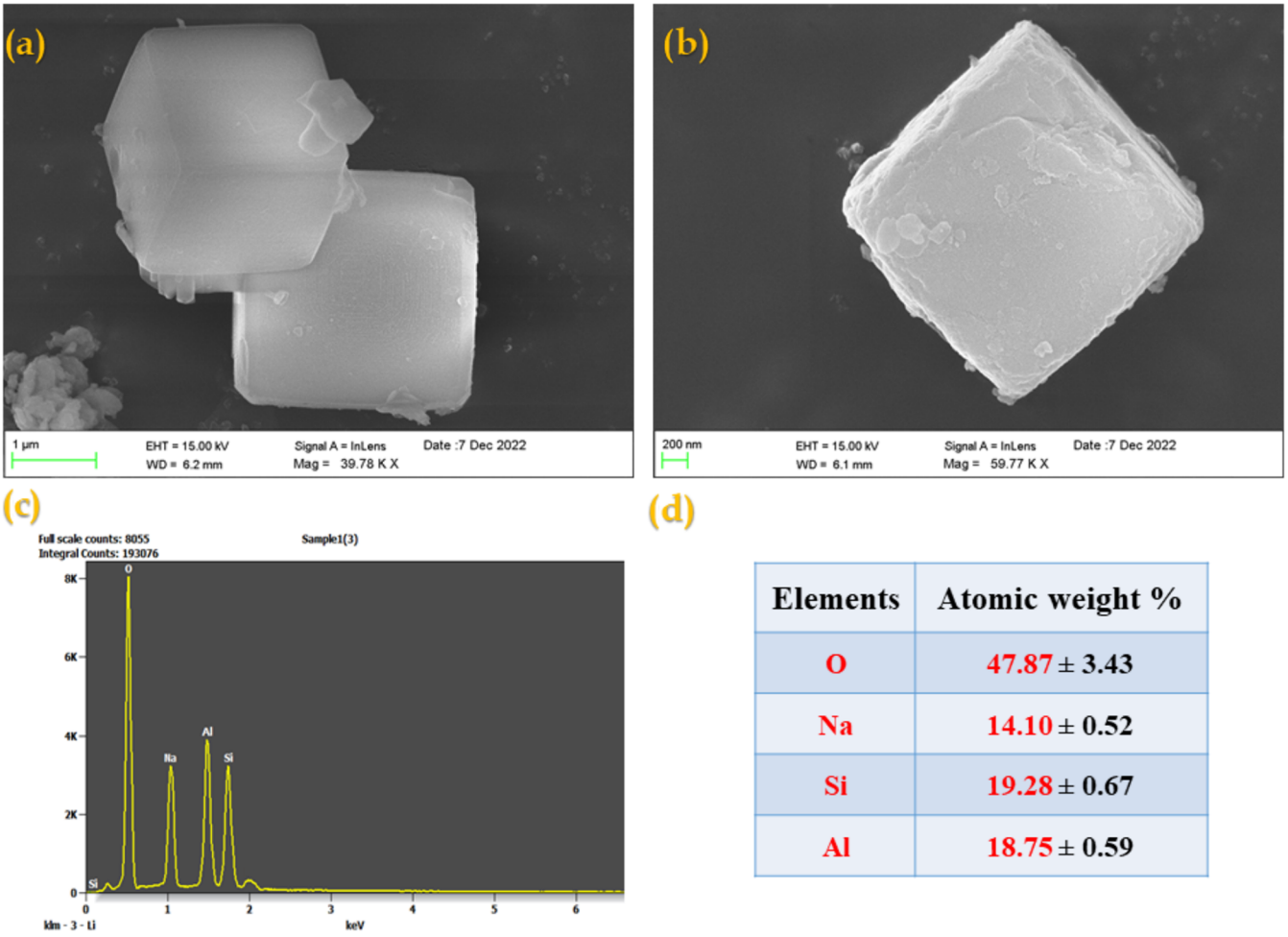

Elements	Atomic weight %
O	47.87 ± 3.43
Na	14.10 ± 0.52
Si	19.28 ± 0.67
Al	18.75 ± 0.59

Figure 6. (a, b) FESEM morphology at two magnifications (c) EDAX spectrum and (d) Elemental composition of the prepared zeolite A type.

have peaks at 2θ = 7.3, 10.2, 12.5, 16.1, 20.4, 21.6, 23.9, 26.1, 27.1, 29.8, 30.8, 32.5, 34.1, 42.2, and 44.1°. The sharp peaks show the crystalline nature of the materials, and they match well with the International Centre for Diffraction Data (ICDD) card number 39-0222, $Na_{96}Al_{96}Si_{96}O_{96}{\cdot}216H_2O \sim Si/Al/Na = 1:1:1$. The lattice parameters and space group of the zeolite A type are found to be $a = b = c = 24.61$ Å and $Fm\bar{3}c$ respectively. Also, the obtained zeolites belong to face centered cubic structure, similar results have been studied by earlier workers.[25,26]

From the obtained results, it is observed that compared to the peaks of parent NaA zeolite, the ion exchanged zeolite peaks show different intensities, indicating that Cu^{2+} ions are predominantly deposited in distinct areas of zeolite. It has also been reported by Yao et al.[27] and Benaliouche et al.[28] that the intensity of the zeolite characteristic peaks decreases as the concentration of Cu^{2+} is increased. Hence, the decrease in peak intensity as the degree of exchange increases suggests a reduction of crystallinity. The size and charge of exchangeable cations play a significant role in altering the zeolite framework during the exchange process.[29]

The crystallite size value of both prepared and ion exchanged zeolites is calculated by using Debye−Scherrer's relation. The average crystallite size value of the prepared zeolite A and ion exchanged zeolite (C1−C4) has been calculated and is given in the Table S1.

3.2. Fourier Transform Infrared Spectroscopy (FTIR) Analysis. FTIR spectroscopy is employed to analyze the functional group in materials. Each functional group exhibits a unique vibrational energy, allowing for the identification of molecules. Additionally, it is an efficient tool for analyzing the zeolite framework structure. The FTIR spectra of the prepared and ion exchanged zeolite are given in Figure 3a−e.

In Figure 3a, the vibrational band at 3354 cm^{-1} is linked to the OH stretching vibration. The band at 1641 cm^{-1} corresponds to the scissor-type bending vibration of the adsorbed water molecules. According to Hassan and Hameed,[30] the presence of water molecules in zeolite is responsible for bands between 1600 and 3700 cm^{-1}. The asymmetrical stretching υ(as) band at 966 cm^{-1} is associated with T−O bonds, where T denotes the tetrahedron of the zeolite framework material (T = Si or Al).[31,32] The band at 667 cm^{-1} is due to the internal vibration of the Al−O−Si symmetrical stretching υ(s). The 551 cm^{-1} band is attributed to a D4R vibration, resulting from the interaction between the υ(s) vibrations of silicon and aluminoxy tetrahedra, which form the SBU of zeolite A type, as also reported by earlier reports.[33] The band at 468 cm^{-1} is attributed to the Si−O−Si bending vibration of the zeolite.

Similarly, in Figure 3b−e for Cu^{2+} ion-exchanged zeolites, the band at 3404 cm^{-1} corresponds to the OH stretching vibration. The band at 1648 cm^{-1} is associated with the scissor-type bending vibration of water molecules, consistent with previous studies.[26,34] The band at 977 cm^{-1} indicates the υ(as) characteristic internal vibration of the T−O bonds. where T represents the tetrahedral elements of the zeolite framework,

https://doi.org/10.1021/acsomega.4c05487
ACS Omega 2024, 9, 45926−45942

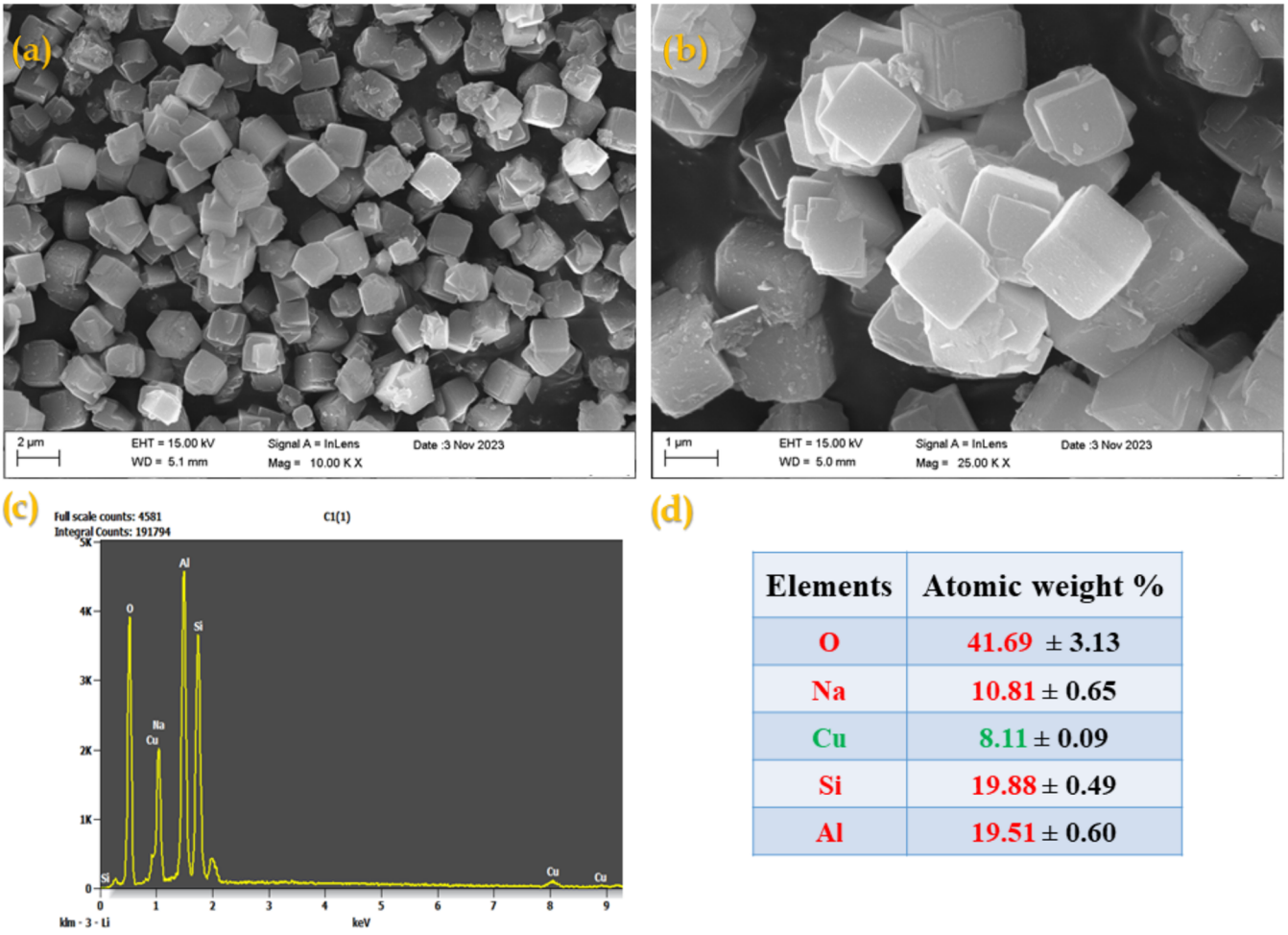

Elements	Atomic weight %
O	41.69 ± 3.13
Na	10.81 ± 0.65
Cu	8.11 ± 0.09
Si	19.88 ± 0.49
Al	19.51 ± 0.60

Figure 7. (a, b) FESEM morphology at two magnifications (c) EDAX spectrum and (d) Elemental composition of the Cu^{2+} ion-exchanged zeolite (C1).

specifically (T = Si or Al).[31] The 663 cm^{-1} band represents the υ(s) of Al−O−Si. The bands at 549 cm^{-1} suggest the presence of D4R, resulting from the interaction between the υ vibrations of silicon and aluminum tetrahedra, which form the SBU of the zeolite structure. It is also noted that the intensity of band present at 549 and 663 cm^{-1} for C3 and C4 zeolites are further reduced compared to other zeolites.[35] The reduction in intensity is due to the presence of the vibration mode of Cu−O obtained during the ion exchange process.[35,36] The band at 463 cm^{-1} corresponds to the Si−O−Si bending vibration of the ion-exchanged zeolite, aligning with the findings of earlier research.[37,38]

For ion exchanged zeolite, the only visible change in the observed spectra is the slight shift of the asymmetrical stretching vibrational band of the T−O band toward the higher wavenumber. Similarly, the shift of Al−O−Si symmetrical stretching toward the lower wavenumber with the increase of ion exchange process, the findings are consistent with previous reports.[39] Correspondingly, the intensity of the bands of the ion exchanged zeolites is less compared to the prepared zeolites and is this due to the removal of Al from the framework which leads to the formation of an additional framework of Al species and condensation of silanol groups.[38] Hence, this results in a frequency shift and a reduction in intensity for the ion exchanged zeolites. The vibrational spectral values and their associated functional groups are consistent with those published in literature.[26,34,37]

3.3. Thermal Analysis. Thermal analysis is utilized to explore the thermal properties, such as mass loss, thermal stability, and structural changes, of the prepared zeolite samples under a nitrogen atmosphere at elevated temperatures. During the analysis of prepared and ion exchanged zeolites, two forms of weight loss were observed. The primary cause of mass loss is the release of water molecules from the zeolite framework structure. This loss occurs at lower temperatures, typically between 100 and 150 °C, and this is attributed to the removal of surface and cavity-bound moisture. Mass loss at elevated temperatures results from the removal of water molecules present between adjacent framework molecules without significantly altering the structure. Figures 4 and 5(a and b) depict the Thermogravimetric/Differential thermal analysis (TG/DTG) analysis of both prepared and Cu^{2+} ion-exchanged zeolites, conducted at temperatures ranging from 25 to 950 °C under N_2 atmosphere.

The TG curve obtained from thermogravimetric analysis illustrates the hydration behavior of the synthesized zeolites, showing a consistent loss of water molecules with increasing temperature. Both synthesized and ion-exchanged zeolites experience primary mass loss starting at around 30 °C and continuing up to approximately 200 °C. This initial loss is attributed to the evaporation of water and volatiles present within the pores. Figures 4 and 5(a) indicate a mass loss in the

https://doi.org/10.1021/acsomega.4c05487
ACS Omega 2024, 9, 45926−45942

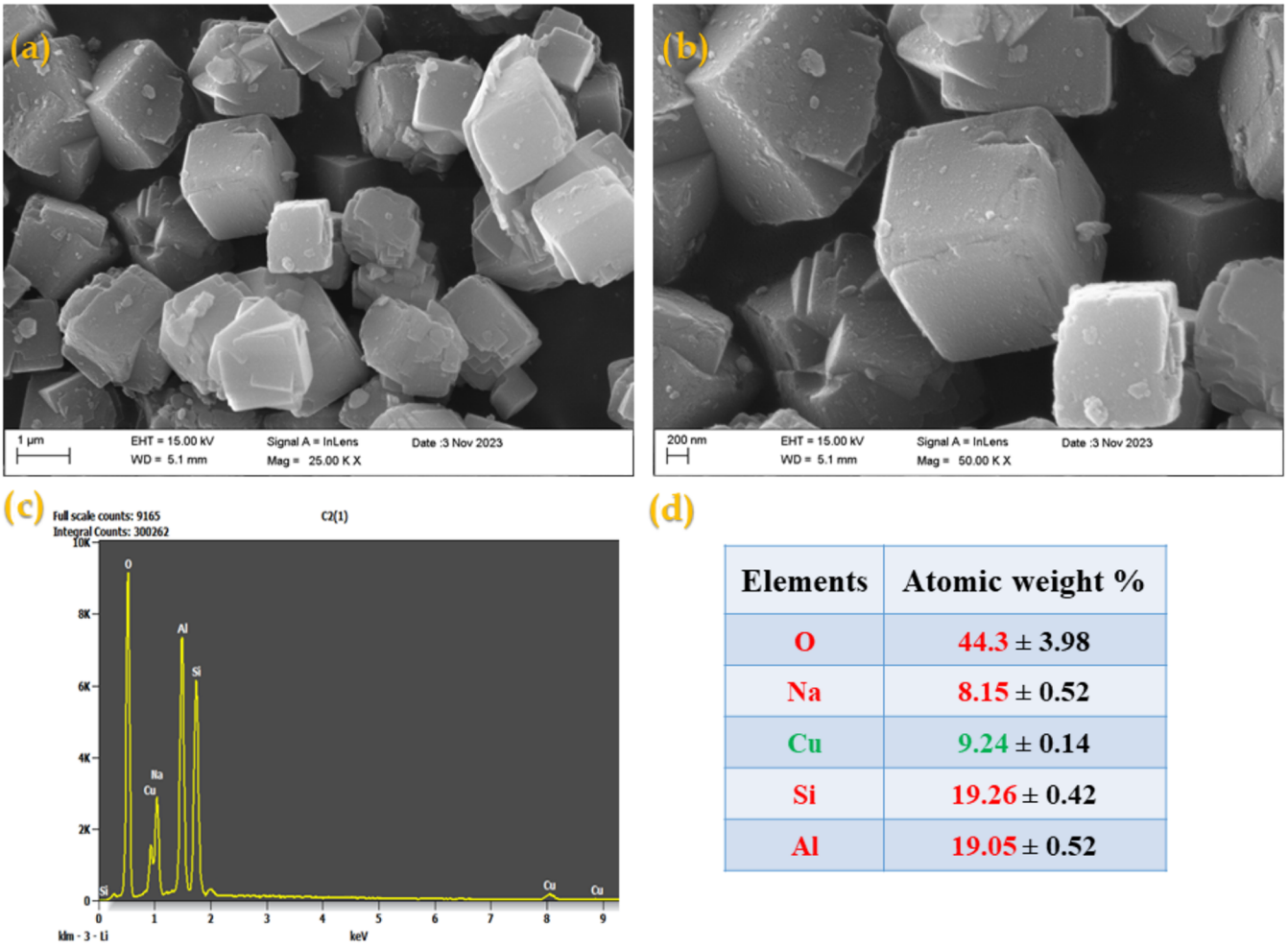

Elements	Atomic weight %
O	44.3 ± 3.98
Na	8.15 ± 0.52
Cu	9.24 ± 0.14
Si	19.26 ± 0.42
Al	19.05 ± 0.52

Figure 8. (a, b) FESEM morphology at two magnifications (c) EDAX spectrum & (d) Elemental composition of the Cu^{2+} ion-exchanged zeolite (C2).

temperature range of 15−17%. The mass loss during this phase is primarily because of the removal of water molecules from various energy levels within the zeolite lattice structure. This process is influenced by the type of coordinated cations present, consistent with the earlier findings.[40] Beyond 200 °C, mass loss in both prepared and ion-exchanged zeolites is primarily due to the loss of moisture. At temperatures exceeding 600 °C, mass loss occurs gradually as water molecules strongly bound to the sodalite cages are removed, in line with earlier research.[41]

Figure 4 displays the DTG curve of the prepared zeolite, while Figure 5a shows those of the ion-exchanged zeolites. The desorption peak for the synthesized zeolite is approximately 156 °C, whereas for Cu^{2+} ion-exchanged zeolites, it occurs around 146 °C. The variation in loss is due to the type of coordinated cations within the produced zeolite and is consistent with previous findings.[42] The presence of a single water desorption peak in both the synthesized and ion-exchanged zeolites suggests a singular bonding form, indicating a specific type of water grafting loss within the zeolite material.[40] At elevated temperatures, the maximum loss is observed to be approximately 1−2.5% for both synthesized and ion-exchanged zeolites, indicating structural stability, resulting in the expulsion of additional water molecules from the zeolite framework cavities as similar results have been reported by earlier workers.[41,43]

Figure 4 illustrates the DTA of the prepared zeolite, while Figure 5b displays those of the ion-exchanged zeolites. The endothermic region observed in the range of 100−200 °C indicates the early desorption of physisorbed water, leading to the emergence of the anhydrous phase. At around 400 °C, the nature of the curve reflects the elimination of trapped water molecules from the zeolite cages.[31,43] Additionally, the curve displays a slight weight loss above 500 °C, indicating the final stage of zeolite dehydration, with stabilization occurring around 700 °C. The exothermic region at higher temperatures provides insight into the thermal stability of the prepared zeolites. An exothermal peak observed in the range of approximately 760−800 °C suggests the collapse of the synthesized material framework structure. It is worth noting that the heat resistant strength of the prepared materials correlates directly with the Si/Al ratio of the zeolites. The Si/Al ratio of both prepared and ion exchanged zeolites is identified by using energy dispersive X-ray analysis (EDAX) spectra and is consistent with the reported results.[43]

3.4. Field Emission Scanning Electron Microscopy (FESEM) and Energy Dispersive X-ray Analysis (EDAX). FESEM analysis is employed to examine the morphology and particle size of both prepared and ion-exchanged zeolites. Figures 6−10(a−d) display FESEM images of prepared and ion exchanged materials at various magnifications. Two specific micrographs are selected to highlight the morphology of each synthesized and ion-exchanged zeolite. In Figure 6a,b, the FESEM images of prepared zeolites reveal an "Ice cube" shaped morphology. This morphology is attributed to the interconnection of sodalite cage secondary building units (SBUs) via D4R,

https://doi.org/10.1021/acsomega.4c05487
ACS Omega 2024, 9, 45926−45942

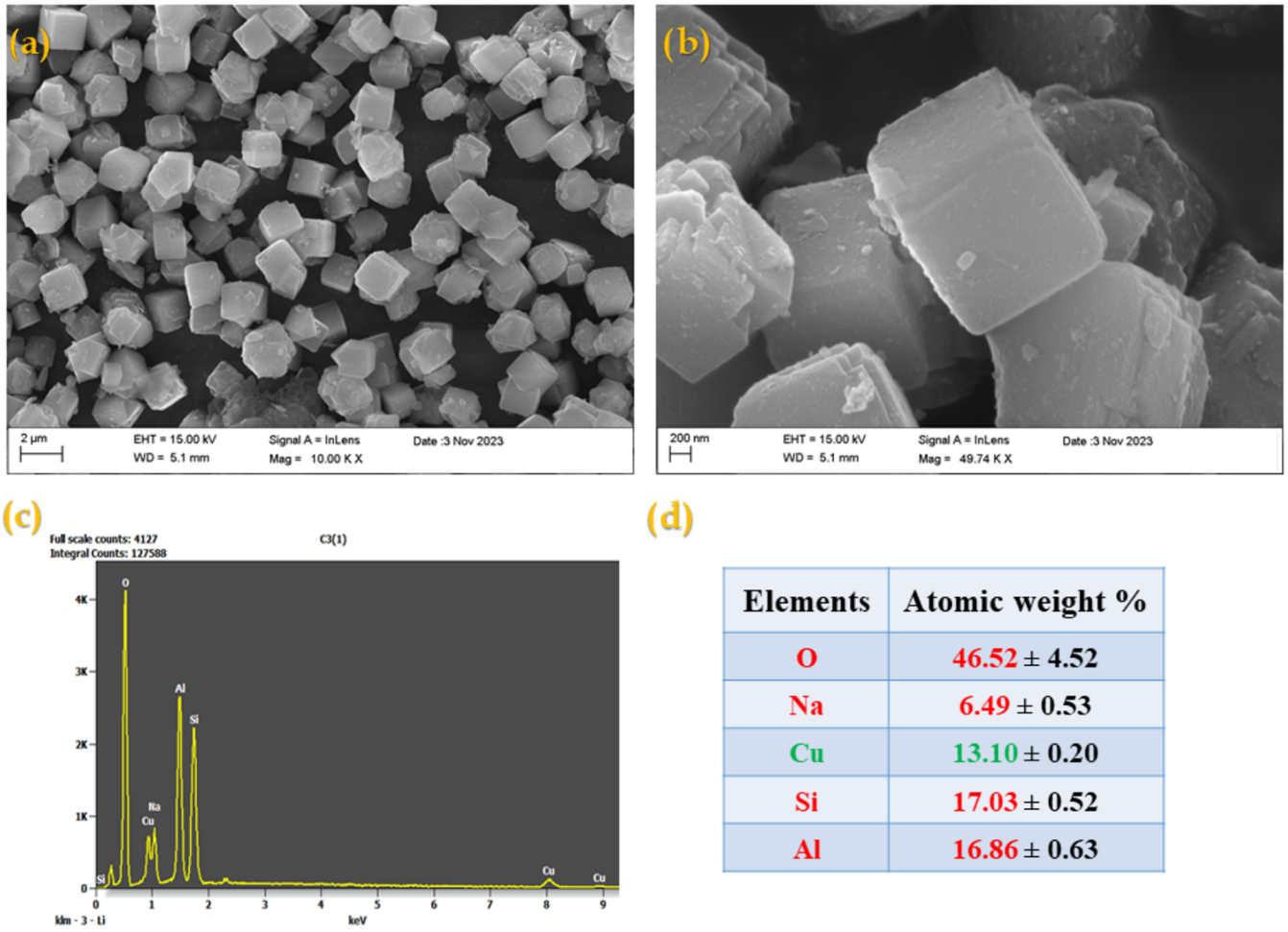

Elements	Atomic weight %
O	46.52 ± 4.52
Na	6.49 ± 0.53
Cu	13.10 ± 0.20
Si	17.03 ± 0.52
Al	16.86 ± 0.63

Figure 9. (a, b) FESEM morphology at two magnifications (c) EDAX spectrum and (d) Elemental composition of the Cu^{2+} ion-exchanged zeolite (C3).

resulting in a three-dimensional micropore cubic structure (α-cage), and is consistent with previous findings.[44] The particle size of the prepared zeolites lies between 1.8 to 2.1 μm, with an average size of 2 μm.

Similarly, Figures 7−10(a,b) represent the FESEM images of the Cu^{2+} ion exchanged zeolites at two different magnifications. According to micrographs, the guest ions (Cu^{2+} replacing Na^{+}) incorporated in the zeolite morphology are found to be identical to synthesized zeolites. Even after ion exchange with ternary Cu^{2+} the morphology shows a nearly identical look, demonstrating that the zeolite structure is unaffected, and this is in agreement with the reported result.[45] For ion exchange zeolite, it is found that their particle sizes lie between 1 and 2 μm. While the majority of the ion-exchanged zeolites preserved their typical morphologies even after the ion-exchange process but there are tiny changes like the presence of some broken crystals.[31,46]

Figures 6−10(c) present the EDAX spectra of both synthesized and ion-exchanged zeolites. Analysis of these spectra reveals the presence of elements such as sodium, oxygen, silicon, and aluminum in the prepared zeolite. Copper, sodium, oxygen, silicon, and aluminum are present in Cu^{2+} ion-exchanged zeolites, consistent with prior studies. The error percentage in EDAX measurements was calculated using the ZAF correction method to account for atomic number effects, X-ray absorption, and fluorescence interactions, as described in the literature Goldstein et al.,[47] and Williams and Carter[48] for ensuring accurate elemental quantification. The original FESEM images utilized for the EDAX data analysis are provided in Figure S1a−e. Chemical composition data for both prepared and ion-exchanged zeolites are shown in Figures 6−10(d). The Si/Al ratio is a critical factor in the zeolite synthesis process. For both prepared zeolite A and ion exchanged zeolites (C1−C4) they have nearly reached saturation in aluminum content within their framework compositions, with a Si/Al molar ratio close to one. This ratio represents the maximum aluminum content allowable in tetrahedral aluminosilicate frameworks, adhering to Loewenstein's rule.[49,50] As a result, they possess the maximum number of cation exchange sites to balance the framework aluminum, resulting in the highest cation contents and exchange capacities. The obtained results are in agreement with the previously reported results.[50,51]

Elemental mapping of the prepared and ion-exchanged zeolites are provided in Figures S2−S6. Zeolite A type typically exhibits an average Si/Al ratio of ≤1. The Si/Al ratio for prepared zeolite A type is found to be 1.02 and for ion exchanged zeolites (C1−C4) it is found to be 1.01, 1.01, 1.01, and 1.02 respectively. For both prepared and Cu^{2+} ion-exchanged zeolites, the obtained Si/Al ratio was approximately 1.

3.5. N_2 Adsorption/Desorption Studies. By using the Brunauer−Emmett−Teller (BET) method, the materials surface area and pore size were determined by measuring the volume of N_2 gas adsorption and desorption at a constant liquid

https://doi.org/10.1021/acsomega.4c05487
ACS Omega 2024, 9, 45926−45942

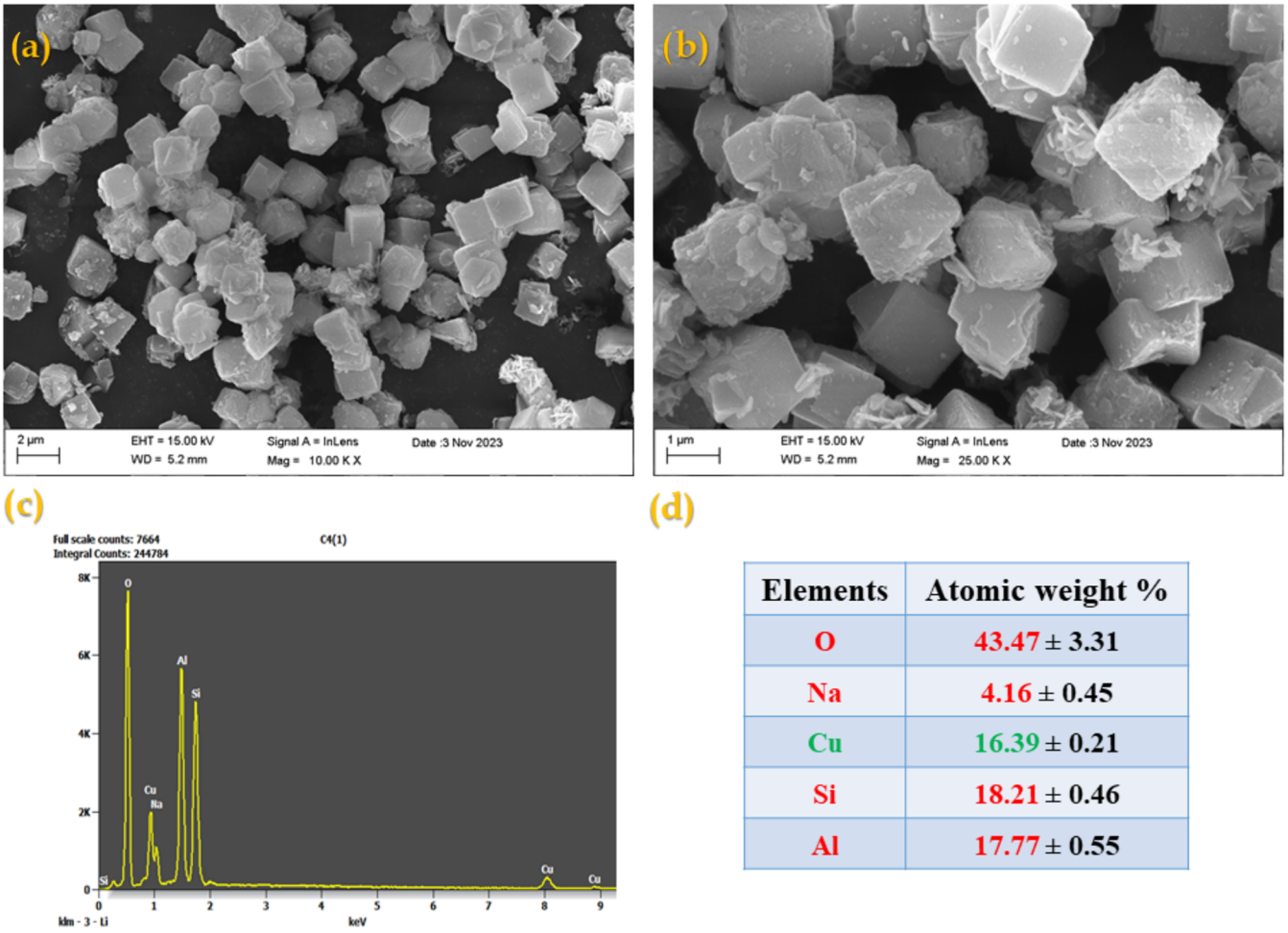

Elements	Atomic weight %
O	43.47 ± 3.31
Na	4.16 ± 0.45
Cu	16.39 ± 0.21
Si	18.21 ± 0.46
Al	17.77 ± 0.55

Figure 10. (a, b) FESEM morphology at two magnifications (c) EDAX spectrum and (d) Elemental composition of the Cu^{2+} ion exchanged zeolite (C4).

N_2 state of −196 °C (77 K).[52] Figure 11a illustrate the N_2 adsorption/desorption isotherm studies of both prepared and Cu^{2+} ion-exchanged zeolites. At low relative pressure, because of the strong contact between the adsorbent and adsorbate, the ion-exchanged zeolites display much stronger N_2 adsorption. N_2 molecules are predominantly present at the pore openings of the zeolite framework structure.[53]

The prepared and ion-exchanged zeolites (C1−C4) displays a type IV adsorption isotherm accompanied by an H3 hysteresis loop, consistent with IUPAC classification criteria.[25,54] Thus, the isotherm results confirm the mesoporous nature of the synthesized material. The presence of smaller pore sizes (4 Å) in the synthesized zeolites indicates microporosity at low pressure regions (P/P_o = 0.01).

Additionally, the presence of a slit-shaped curve denotes the H3 hysteresis loop in the region between 0.4 < P/P_o < 0.9, and this is attributed to the filling of the mesoporous region within the zeolite framework, similar results have been reported by earlier workers.[31,55] The emergence of a weak desorption hysteresis loop curve is attributed at high relative pressures (P/P_o > 0.9), indicating the coexistence of micropores and mesopores within the zeolite framework structure.

The BET surface area of about 96.12 m^2/g is observed for the synthesized zeolite. Similarly, for the different Cu^{2+} ion incorporated zeolites, BET surface areas of 81.92, 133.16, 116.14, and 90.63 m^2/g, were obtained for (C1−C4) ion exchanged zeolites. In comparison to synthesized zeolite A and other ion exchanged zeolites, the 0.1 M Cu^{2+} ion exchanged zeolite has a larger surface area because of the presence of fewer Na^+ cations per unit cell in its pores, resulting in a relatively greater BET surface area. The ion exchange process leads to an expansion of the zeolite structure, creating more surface area that is available for adsorption. As the concentration Cu^{2+} increases more than 0.1 M, it results in pore blockage and/or mesopore formation as stated in the literature.[25] Due to its high concentration of Na^+ cations and low Si/Al ratio, the synthesized zeolite A type has a small BET surface area compared to ion-exchanged zeolites as N_2 is not able to enter most of the micropores.

Figure 11b shows the pore size distribution (PSD) of both prepared zeolite and Cu^{2+} ion-exchanged zeolites. The PSD of prepared zeolites is determined using the BJH equation. According to IUPAC classification criteria, pores with diameters less than 2 nm are classified as microporous, the pores present in the region between 2 to 50 nm are considered as mesoporous, and those exceeding 50 nm fall into the macroporous category. Figure 11b illustrates the PSD of the prepared zeolite, with an average pore size found to be about 4.79 nm. Also, the PSD of the Cu^{2+} ion-exchanged zeolites with an average size of 4.24, 4.17, 4.69, and 4.73 for C1, C2, C3, and C4, respectively. The pore size distribution depicted in Figure 11b reveals that the samples exhibited a multimodal distribution of mesopores

https://doi.org/10.1021/acsomega.4c05487
ACS Omega 2024, 9, 45926−45942

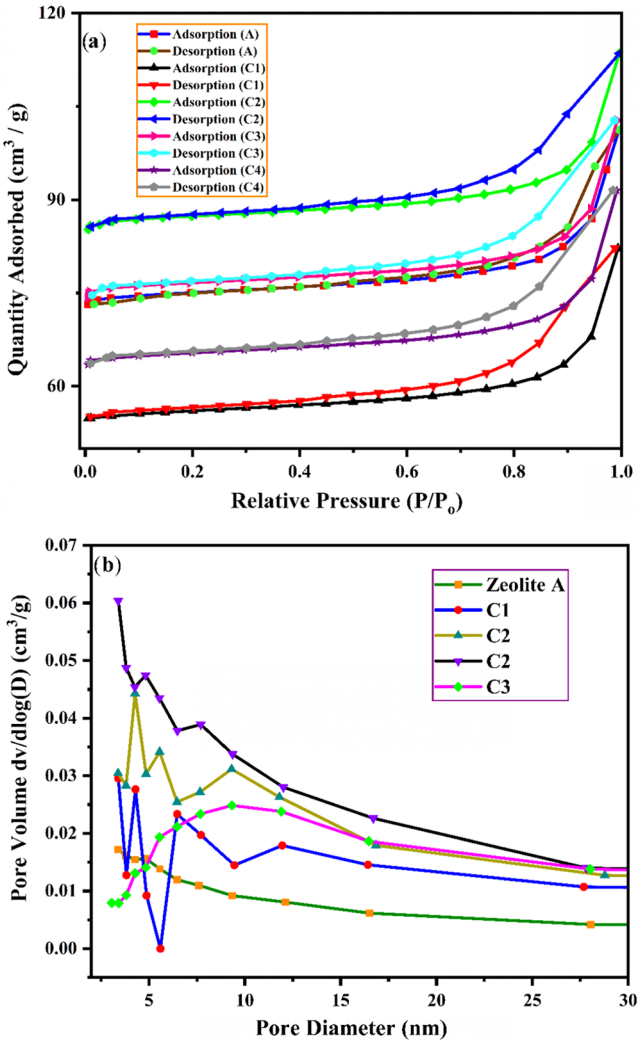

Figure 11. (a) N_2 adsorption/desorption isotherm and (b) Pore size distribution (PSD) of prepared zeolite A type and ion-exchanged zeolites (C1−C4).

within the small-size range of 3 to 13 nm, similar results have been reported by earlier workers.[43,56] After the addition of copper species into the zeolite framework, the pore structure of the material was not greatly altered. The appearance of the characteristic H3 hysteresis loop is associated with the presence of irregular meso- or micropores formed during the ion exchange process. Limited access of Cu^{2+} ions to the zeolite pores can lead to channel distortion.[57] Some investigations have highlighted the fact that one Cu^{2+} ion replaces two Na^+ ions during ion exchange.[25,57] The channels may become distorted as a result of the Cu^{2+} ions having a limited accessibility to the zeolite pores. The ion-exchanged zeolite shows an increase in micropores to multimodal mesoporous region, leading to a more complex distribution of adsorption surface energy. This modification in porosity is attributed to variations in the type and quantity of cations within the zeolite structure.[16] As a result, the higher concentration of ion-exchange zeolites significantly affects the S_{BET} surface.[58] The comparison of textural properties of the prepared and Cu^{2+} ion exchanged A type zeolites are given in Table 1.

3.6. CO_2 Adsorption Studies. The pore size of a material and the strength of the gas−solid interaction are critical factors in determining the gas adsorption capacity. This interaction

Table 1. Comparison of Textural Properties of Both Prepared Zeolite A Type and Cu^{2+} Ion-Exchanged Zeolites with Previously Reported Zeolite Materials

Materials	BET surface area (S_{BET}) (m^2/g)	Micropore volume (cm^3/g)	References
Zeolite/Chitosan (1:3:5)	7.0	0.030	59
Zeolite/Chitosan (1:3:5)	0.5	0.003	59
Zeolite KA	0.26 ± 0.07		60
Zeolite RbA	0.95 ± 0.06		60
Zeolite CsA	0.47 ± 0.07		60
Zeolite Li-SSZ-13	27	0.27	61
Zeolite Na-SSZ-13	7	0.24	61
Zeolite K-SSZ-13	65	0.18	61
Zeolite LTA −0.5	72.42	0.328	62
Zeolite A	58.29	0.071	31
Zeolite CAN	59.09	0.101	63
Zeolite A	5.16	0.006	64
Zeolite A	39	0.016	65
Zeolite A	96.12	0.231	this work
Zeolite C1	81.92	0.196	this work
Zeolite C2	133.16	0.331	this work
Zeolite C3	116.74	0.291	this work
Zeolite C4	90. 63	0.214	this work

strength is explored through the pore structure, surface chemistry, and other properties of the adsorbent, such as polarizability, molecular size, and quadrupole moments. For instance, the polarizability of a CO_2 molecule is approximately 26.5×10^{-25} cm^3, while its quadrupole moment is about 4.3×10^{-26} esu cm^2 respectively.[66] Figures 12−16(a) illustrates the CO_2 adsorption/desorption properties of both synthesized and ion-exchanged zeolites at a steady temperature of 297.15 K, covering a pressure range from 0 to 1 bar, respectively.

The adsorption curves of both prepared and ion-exchanged zeolites exhibit a type I adsorption isotherm, consistent with the IUPAC classification criteria. The maximum adsorption capacity is measured as 2.14 mmol/g for the synthesized sample. Similarly, for Cu^{2+} zeolites (C1, C2, C3, & C4), the observed capacities are 2.58, 4.02, 3.19, and 2.78 mmol/g, respectively. In the low-pressure region, a sharp gradient is observed due to high adsorption, while at higher pressures, this gradient gradually decreases, and the isotherm curve flattens out toward saturation. CO_2 molecule adsorption by zeolites is attributed to significant quadrupolar interactions among the adsorbate molecules and the gradient electric field generated by the charge-balancing cation of zeolite structure.[43,67−69]

It is noteworthy to mention that the cations located in the Primary building blocks unit (PBU) can readily interact with guest molecules, in contrast to those situated in the double 4-ring cavities (SBU). The exchangeable vacant cations that occupy positions within this PBU framework are considered extra-framework cations.[67] In summary, the cations (Na^+ and Cu^{2+} ions) can reduce the acidity and enhance the basicity of the zeolite framework, which is advantageous for the adsorption of acidic CO_2.[67,70]

In the zeolite structure, some of the Si atoms can be replaced by other elements, with Al being the most favorable alternative. A negatively charged framework is produced when Al (oxidation state +3) is present rather than Si (+4). The presence of extra-framework counter-cations (such as Na^+ and Cu^{2+}) balances out

https://doi.org/10.1021/acsomega.4c05487
ACS Omega 2024, 9, 45926−45942

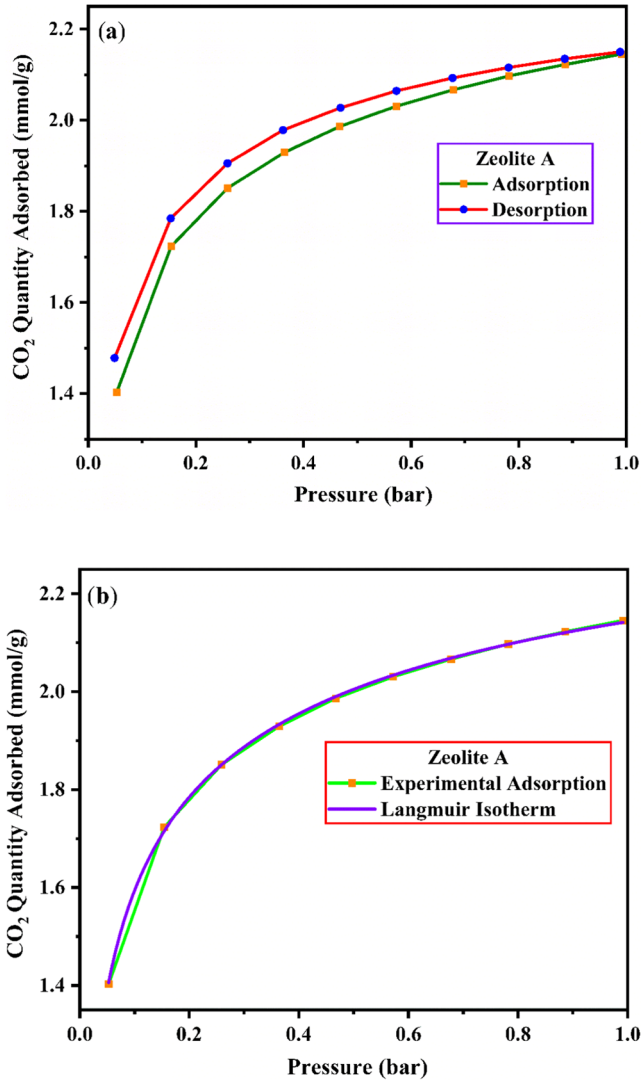

Figure 12. (a) Experimental CO_2 adsorption/desorption isotherms of prepared zeolite A type at 297.15 K and (b) Fitted Langmuir adsorption isotherm with experimental CO_2 adsorption data.

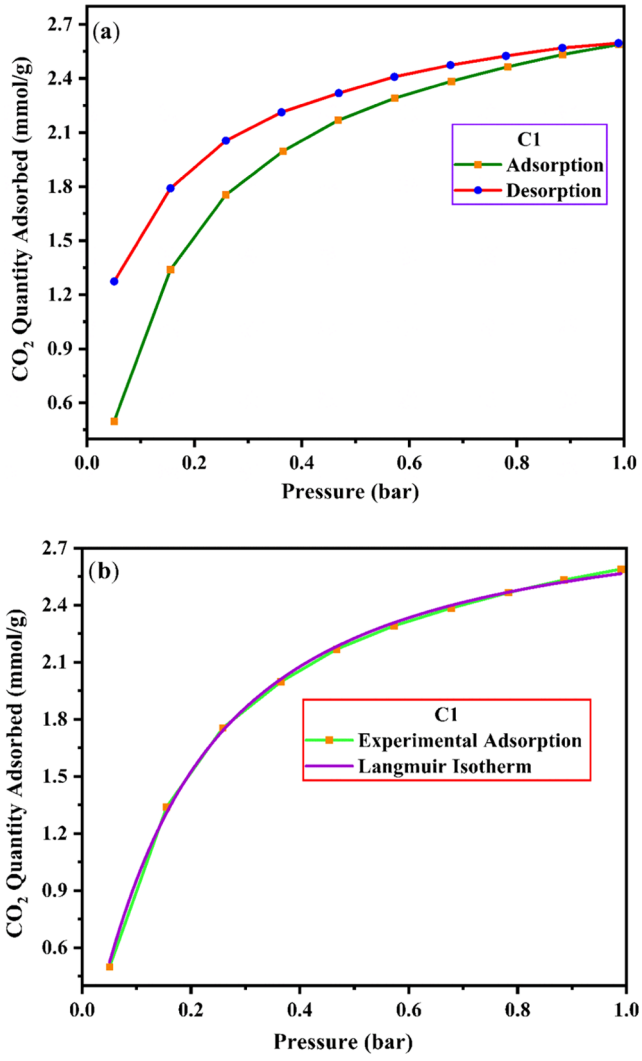

Figure 13. (a) Experimental CO_2 adsorption/desorption isotherms of C1 ion-exchanged zeolite at 297.15 K and (b) Fitted Langmuir adsorption isotherm with experimental CO_2 adsorption data.

these negative charges.[71] The CO_2 adsorption isotherm exhibits a rapid rise at low relative pressure due to the significant electrostatic interaction between CO_2 quadrupoles and vacant cations within the zeolite material framework. Saturation occurs at high relative pressure, where the isotherm curve reaches a plateau, indicating the absence of free vacant cations in the framework structure.[67]

The adsorption mechanisms for CO_2 using synthesized and ion-exchanged zeolites commonly involve two scenarios: (i) One oxygen atom of CO_2 interacts with an extra-framework cation of zeolites, and (ii) Both oxygen atoms of CO_2 interact with multiple extra-framework cations of the zeolite structure through a bridging mechanism. The interaction between the CO_2 molecules and the Na^+/Cu^{2+} cation in the extra-framework structure is primarily driven by ion-dipole interactions. Consequently, the adsorption of adsorbate molecules is facilitated by vacant alkali cations (such as Na^+ and Cu^{2+}) present in the synthesized and ion-exchanged zeolite framework structure.[72]

The results indicate that the 0.1 M Cu^{2+} ion-exchanged zeolite exhibits maximum CO_2 adsorption compared to those of other prepared and ion-exchanged zeolites. This is because the 0.1 M Cu^{2+} ion-exchanged zeolite contains a larger number of alkali cations capable of interacting with the adsorbate molecules. The existence of additional Na^+/Cu^{2+} cations in the zeolite framework enhances its basic nature, leading to greater adsorption of acidic CO_2 molecules. Consequently, the adsorbed molecules accumulate in the pores of the zeolite framework.[43,67]

Zeolite A is a small-pore zeolite composed of sodalite cages that are connected by D4R forming an accessible super cage via an eight-membered ring (8MR). The window of the 8MR provides access to the super cage situated near the alkali cations. The kinetic diameter of ion-exchanged zeolite is about 0.4 nm, which is nearly identical to the diameter of a CO_2 molecule of about 0.33 nm thus resulting in increased adsorption of CO_2.[73] It is evident from Figure 14a that 0.1 M of Cu^{2+} ion-exchanged zeolites show better adsorption compared to the synthesized and other ion-exchanged zeolites. When compared to the other zeolites, the 0.1 M ion-exchanged zeolite has the maximum intake of CO_2 molecules, which may be due to its better surface area and also favorable Si/Al ratio.

https://doi.org/10.1021/acsomega.4c05487
ACS Omega 2024, 9, 45926−45942

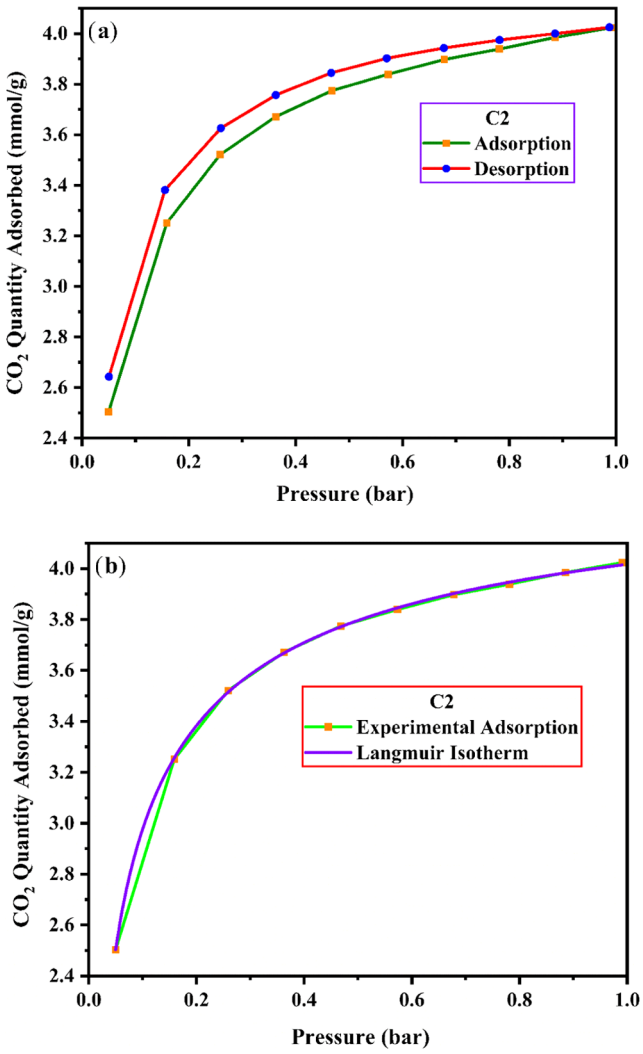

Figure 14. (a) Experimental CO_2 adsorption/desorption isotherms of C2 ion-exchanged zeolite at 297.15 K and (b) Fitted Langmuir adsorption isotherm with experimental CO_2 adsorption data.

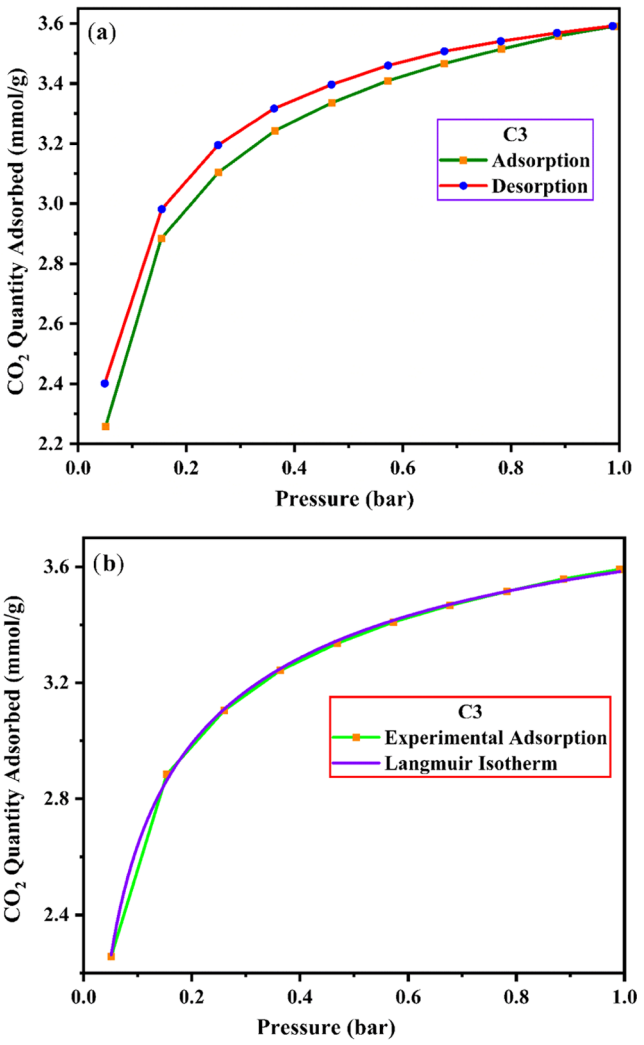

Figure 15. (a) Experimental CO_2 adsorption/desorption isotherms of C3 ion-exchanged zeolite at 297.15 K and (b) Fitted Langmuir adsorption isotherm with experimental CO_2 adsorption data.

The Si/Al ratio obtained from the EDAX spectrum significantly influences the adsorption capacity of CO_2. A lower Si/Al ratio, indicating a higher content of Al, results in the presence of extra-framework cations in zeolites, which are typically active sites for adsorption. This suggests that a lower Si/Al ratio enhances the amount of adsorption per unit mass of the material, thereby improving the CO_2 adsorption capacity.[74] The presence of the cation (Cu^{2+}) in ion-exchanged zeolites helps balance the negative charge created by the Al atom in the framework, leading to an increased level of CO_2 adsorption. The higher surface area and pore volume, along with increased electrostatic field in the 0.1 M Cu^{2+} ion-exchanged zeolite due to the presence of Cu^{2+} cations and a favorable Si/Al ratio, contribute to higher CO_2 adsorption. The interaction between the CO_2 molecules and zeolite metal ions Cu^{2+} in the linear framework is depicted in Figure 17. The primary interaction is an ion-dipole interaction between the adsorbate and the metal cations in the zeolite framework. The adsorption of the CO_2 molecule is driven by the presence of alkali cations Cu^{2+} in the zeolite structure. The CO_2 molecules interact with the metal cation via their oxygen atoms.[70,75]

Typically, desorption isotherms are positioned above adsorption isotherms, as shown in Figures 12−16(a). The desorption isotherm was derived from depressurization conditions following the completion of the adsorption experiment.[76] This hysteresis continues down to zero pressure along the desorption path. A similar low-pressure hysteresis has been observed in CO_2 sorption studies of sodium alumino silicate-Type 4A zeolite at room temperature, under pressures up to 20 bar.[77] This kind of "open" hysteresis loop is generally linked to a change in the sorbent volume, irreversible gas molecule uptake, or chemisorption.[78] The occurrence of an open hysteresis loop for the synthesized zeolite indicates that CO_2 molecules are likely to enter the microporous structure of the material.

The absence of a closed hysteresis loop can be explained by the behavior of the CO_2 molecules during the adsorption process. The CO_2 molecules diffuse into the zeolites until they reach a cation, which acts as a gatekeeper and limits further movement of the materials. During the desorption phase, CO_2 molecules can easily leave the framework, resulting in no significant hysteresis loop was recorded.[77,78]

de Oliveira et al.[79] in their work explained one of the possible explanations for the open hysteresis loop is the partial blockage of the small zeolite pores, which have an effective aperture of 0.43 nm in the sodium form. As a result, the adsorption phase is primarily governed by the α-cages, which have a diameter of

https://doi.org/10.1021/acsomega.4c05487
ACS Omega 2024, 9, 45926−45942

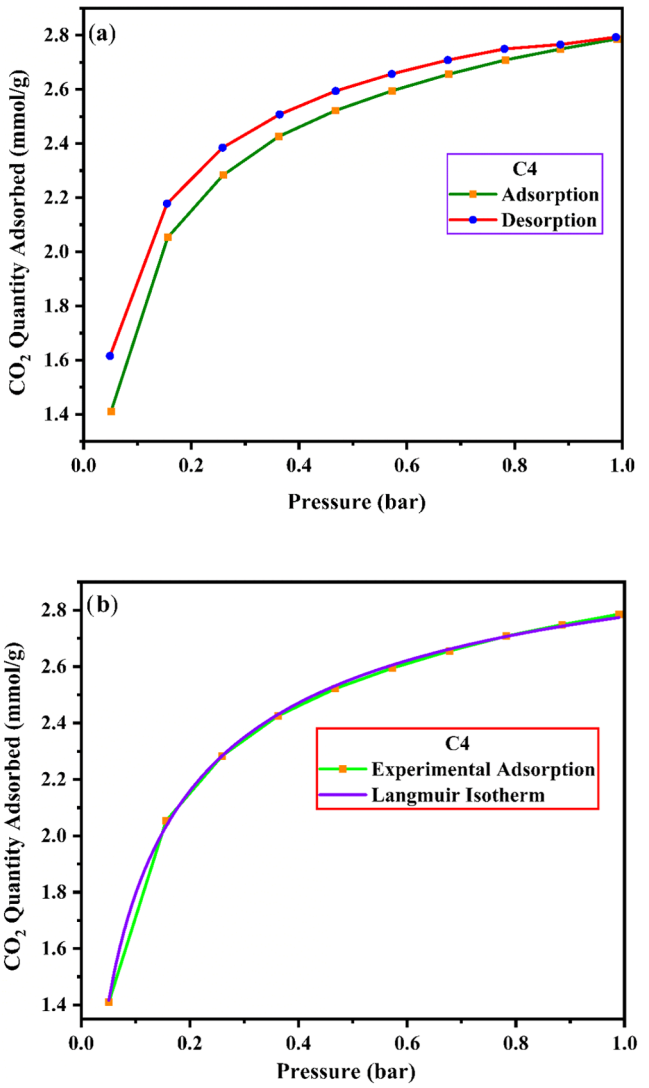

Figure 16. (a) Experimental CO_2 adsorption/desorption isotherm of C4 ion-exchanged zeolite at 297.15 K and (b) Fitted Langmuir adsorption isotherm with experimental CO_2 adsorption data.

approximately 1.14 nm, according to Breck[80] and Giannetto et al.[81] In contrast, the desorption phase is influenced by the effective pore aperture of the zeolite NaA, leading to the open hysteresis loop are observed. The obtained results are in agreement with the previously reported studies.[76,82]

The experimental CO_2 adsorption parameters for both synthesized and ion-exchanged zeolites are presented in Table 2. These parameters were obtained by fitting the experimentally observed data using Langmuir−Friedrich−Toth adsorption isotherm models. Detailed discussion on the nonlinear adsorption isotherm relations can be found in the Supporting Information. The curve fitting was conducted using the Origin program 2024. The experimental data fitted with Langmuir adsorption isotherm are shown in Figures 12−16(b). Likewise,

Table 2. Comparison of Experimental CO_2 Adsorption Capacity of Both Prepared Zeolite A Type and Cu^{2+} Ion-Exchanged Zeolites With Previously Reported Zeolite Materials

Materials	Temperature (K)	CO_2 adsorption (mmol/g)	References
K HXA	298.15	0.5	85
K HXA	273.15	0.7	85
Zeolite NaX	323	0.60	86
Zeolite CaA	323	0.75	86
Zeolite Mn-LTA-3	298	1.87	15
Zeolite Ce-LTA-3	298	2.60	15
Zeolite K-CHA	273.15	2.1	87
Zeolite Cs-Rho	298.15	1.2	88
Zeolite TEPA-ZSM-5	298.15	0.12	89
ZSM-5	298	1.79	89
LTA −0.5	298	0.43	62
Na-LTA-3	298	1.81	90
NaA-RS	273.15	1.46	91
Zeolite NaX-Ca^{2+}	298	1.7	92
Zeolite β	298	1.8	93
Zeolite A	297.15	2.14	this work
Zeolite C1	297.15	2.58	this work
Zeolite C2	297.15	4.02	this work
Zeolite C3	297.15	3.59	this work
Zeolite C4	297.15	2.78	this work

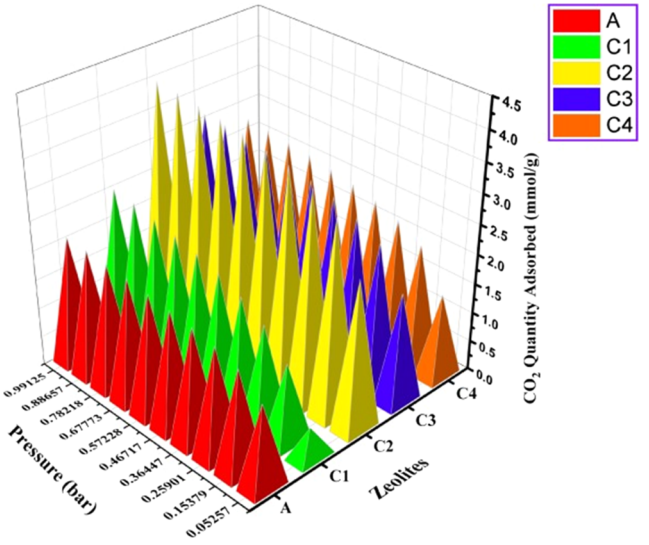

Figure 18. Overall comparison of experimental CO_2 adsorption of both prepared A type and ion-exchanged zeolites (C1−C4).

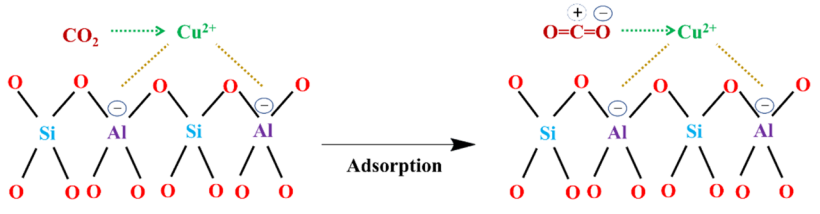

Figure 17. Schematic representation of a possible mechanism for the CO_2 adsorption by ion-exchanged zeolite framework structure.

https://doi.org/10.1021/acsomega.4c05487
ACS Omega 2024, 9, 45926−45942

Table 3. Fitted Adsorption Isotherms Parameter Values of Both Prepared Zeolite A Type and Cu^{2+} Ion-Exchanged Zeolites

	Determined coefficients (R^2)		
Materials	Langmuir adsorption isotherm	Freundlich adsorption isotherm	Toth adsorption isotherm
Zeolite A	0.9997	0.9813	0.9999
Zeolite C1	0.9991	0.9431	0.9981
Zeolite C2	0.9998	0.9550	0.9995
Zeolite C3	0.9995	0.9687	0.9999
Zeolite C4	0.9994	0.9601	0.9995

the experimental CO_2 adsorption data fitted with Freundlich and Toth adsorption isotherm are shown in the Figures S7−S11. It is found from the fitting that the determined coefficients (R^2) are close to 1, indicating a good fit of the experimental data to the model. These results are consistent with previous findings.[68,83] The overall CO_2 adsorption of both prepared A type and ion-exchanged zeolites (C1−C4) is shown in Figure 18. Table 3 presents the parameter values obtained from the fitted isotherms.

Moreover, the pores in both prepared and ion-exchanged zeolite materials are predominantly located in the mesoporous region, as identified by N_2 sorption studies. This positioning may contribute to the development of linear OCO−X^+ complexes, where X^+ represents Na^+ and Cu^{2+} cations. These complexes arise from the interaction between the CO_2 molecules and the zeolite cations. They are also responsible for the perturbation of Si−O−Al bonds during this phase. Size exclusion effects may become more significant in small-pore zeolites and have a specific impact on CO_2 adsorption.[84] In conclusion, the 0.1 M Cu^{2+} ion-exchanged zeolites are observed to adsorb more CO_2 when compared with the synthesized and other ion-exchanged zeolites.

4. CONCLUSIONS

In this work, zeolite A type material has been synthesized through the hydrothermal method. Also, four types of Cu^{2+} ion-exchanged zeolites were synthesized through a cationic ion exchange procedure with Cu concentrations of 0.05, 0.1, 0.15, and 0.2 M. Increasing the concentration of the copper nitrate solution used during ion exchange had a significant impact on the textural and morphological properties of the resulting zeolites. Analysis of the XRD patterns revealed that the intensity of the zeolite A characteristic peak decreases as the concentration of Cu^{2+} increases in ion exchange zeolites. In the FTIR spectra, vibration bands at 551 cm^{-1} were observed for prepared zeolites, while a band at 549 cm^{-1} was observed for Cu^{2+} ion-exchanged zeolites, indicating the presence of D4R and confirming successful zeolite synthesis. The TG analysis showed a mass loss of approximately 15−17% for both the synthesized and ion-exchanged zeolites. FESEM imaging revealed an "ice cube" shaped morphology for the synthesized zeolites. The morphology of Cu^{2+} ion-exchanged zeolites closely resembled that of the prepared zeolites. The EDAX spectrum of Cu^{2+} ion-exchanged zeolites showed the presence of copper elements in addition to sodium, oxygen, silicon, and aluminum elements. The size and charge of the exchangeable cations significantly influence changes in the zeolite framework during the ion exchange process.

N_2 adsorption−desorption studies revealed a type IV adsorption isotherm with an H3 hysteresis loop. Among all zeolites, the maximum BET surface area observed was approximately 133.16 m^2/g for the 0.1 M Cu^{2+} ion-exchanged zeolites. Experimental CO_2 adsorption studies for both synthesized and ion-exchanged zeolites were conducted, revealing a type I adsorption isotherm for synthesized A type and Cu^{2+} ion-exchanged zeolites. The maximum CO_2 adsorption capacity was approximately 4.02 mmol/g for 0.1 M Cu^{2+} ion-exchanged zeolites. The experimental CO_2 adsorption values were fitted using nonlinear adsorption isotherms. Then, the determined coefficients (R^2) for the synthesized and ion-exchanged zeolites were found to be nearly 1, indicating the heterogeneous nature of the materials.

■ ASSOCIATED CONTENT

Data Availability Statement

All data generated or analyzed during this study are included in this published article (and its Supporting Information).

Supporting Information

The Supporting Information is available free of charge at https://pubs.acs.org/doi/10.1021/acsomega.4c05487.

Materials and chemicals, characterization techniques, gas adsorption measurements, nonlinear adsorption isotherm equation, Debye−Scherrer's equation with calculated average crystallite size, FESEM images accompanied by EDAX data of prepared zeolite A type and also for Cu^{2+} ion-exchanged zeolites (C1−C4), elemental mapping of all synthesized zeolites, fitted experimental CO_2 adsorption data with Freundlich and Toth adsorption isotherm for prepared zeolite A type and also for Cu^{2+} ion-exchanged zeolites (C1−C4) (PDF)

■ AUTHOR INFORMATION

Corresponding Author

Jayaprakash Madhu − *Department of Physics, Coimbatore Institute of Technology, Coimbatore, Tamil Nadu 641014, India;* orcid.org/0000-0002-0416-0824; Email: jayaprakashh.madhu@gmail.com

Authors

Agilan Santhanam − *Department of Physics, Coimbatore Institute of Technology, Coimbatore, Tamil Nadu 641014, India*

Dhayalan Velauthapillai − *Faculty of Engineering and Science, Western Norway University of Applied Sciences, 5020 Bergen, Norway;* orcid.org/0000-0002-4162-7446

Complete contact information is available at: https://pubs.acs.org/10.1021/acsomega.4c05487

Author Contributions

J.M. conducted the experimental work for sample preparation and contributed to the manuscript preparation. A.S. and D.V. supervised the work and reviewed the manuscript.

Notes

The authors declare no competing financial interest.

■ ACKNOWLEDGMENTS

The authors gratefully acknowledge the financial support from the Western Norway University of Applied Sciences, Bergen, Norway under the Indo-Norwegian Collaborative Project (INCP 2021-2025), Project No. UTF-2020/10053, funded by

Diku (The Norwegian Agency for International Cooperation and Quality Enhancement in Higher Education).

REFERENCES

(1) Anwar, M. N.; Fayyaz, A.; Sohail, N. F.; Khokhar, M. F.; Baqar, M.; Khan, W. D.; Rasool, K.; Rehan, M.; Nizami, A. S. CO2 capture and storage: A way forward for sustainable environment. *J. Environ. Manage.* **2018**, *226*, 131−144. Cavallo, M.; Dosa, M.; Porcaro, N. G.; Bonino, F.; Piumetti, M.; Crocellà, V. Shaped natural and synthetic zeolites for CO2 capture in a wide temperature range. *J. CO2 Util.* **2023**, *67*, No. 102335.

(2) Gao, W.; Liang, S.; Wang, R.; Jiang, Q.; Zhang, Y.; Zheng, Q.; Xie, B.; Toe, C. Y.; Zhu, X.; Wang, J.; et al. Industrial carbon dioxide capture and utilization: state of the art and future challenges. *Chem. Soc. Rev.* **2020**, *49* (23), 8584−8686.

(3) Sun, S.; Sun, H.; Williams, P. T.; Wu, C. Recent advances in integrated CO2 capture and utilization: a review. *Sustainable Energy Fuels* **2021**, *5* (18), 4546−4559.

(4) Raganati, F.; Miccio, F.; Ammendola, P. Adsorption of Carbon Dioxide for Post-combustion Capture: A Review. *Energy Fuels* **2021**, *35* (16), 12845−12868.

(5) Agency, I. E. *IEA (2020), Global Energy Review 2020*; IEA, Paris. 2020.

(6) Yang, H.; Luo, M.; Chen, X.; Zhao, X.; Lin, J.; Hu, D.; Li, D.; Bu, X.; Feng, P.; Wu, T. Cation-Exchanged Zeolitic Chalcogenides for CO2 Adsorption. *Inorg. Chem.* **2017**, *56* (24), 14999−15005.

(7) Shi, Y.; Liu, Q.; He, Y. CO2 capture using solid sorbents. In *Handbook of Climate Change Mitigation and Adaptation*; Springer New York, 2015; pp 1−56.

(8) Mondal, M. K.; Balsora, H. K.; Varshney, P. Progress and trends in CO2 capture/separation technologies: A review. *Energy* **2012**, *46* (1), 431−441.

(9) Maurya, M.; Singh, J. K. Effect of Ionic Liquid Impregnation in Highly Water-Stable Metal−Organic Frameworks, Covalent Organic Frameworks, and Carbon-Based Adsorbents for Post-combustion Flue Gas Treatment. *Energy Fuels* **2019**, *33* (4), 3421−3428. Xin, C.; Ren, Y.; Zhang, Z.; Liu, L.; Wang, X.; Yang, J. Enhancement of Hydrothermal Stability and CO2 Adsorption of Mg-MOF-74/MCF Composites. *ACS Omega* **2021**, *6* (11), 7739−7745.

(10) Malini, K.; Selvakumar, D.; Kumar, N. S. Activated carbon from biomass: Preparation, factors improving basicity and surface properties for enhanced CO2 capture capacity − A review. *J. CO2 Util.* **2023**, *67*, No. 102318.

(11) Madhu, J.; Vengaipandian, S.; Santhanam, A.; Natarajan, M.; Velauthapillai, D. Adsorption of CO2 Using "Sugar Cube"-Shaped Zeolite A Type Derived from Thermally Treated Kaolin and NaOH. *Energy Fuels* **2023**, *37* (15), 11152−11176.

(12) Dou, X.; Li, W.; Zhang, K.; Hou, H.; He, Z.; Zhu, C.; Meira, D. M.; Lopez-Haro, M.; Xia, Z.; He, P.; et al. Size-Dependent Structural Features of Subnanometer PtSn Catalysts Encapsulated in Zeolite for Alkane Dehydrogenation. *ACS Catal.* **2024**, *14* (5), 2859−2871. Fan, J.; Yao, J.; Feng, X.; Wang, C.; Shi, Y.; Feng, H.; Gao, W.; He, Y.; Guo, X.; Yasuda, S.; et al. Unveiling the Catalytic Role of Zeolite P1 in Carbonylation Reaction. *Chem. Bio Eng.* **2024**, *1* (2), 141−149.

(13) Yashnik, S. A.; Surovtsova, T. A.; Salnikov, A. V. Cu-ZSM-5 catalyst synthesis via ion-exchange with ammonia solution of copper hydroxysalts. *Microporous Mesoporous Mater.* **2024**, *367*, No. 112966.

(14) Ren, Z.; Wang, L.; Li, Y.; Zha, J.; Tian, G.; Wang, F.; Zhang, H.; Liang, J. Synthesis of zeolites by in-situ conversion of geopolymers and their performance of heavy metal ion removal in wastewater:A review. *J. Cleaner Prod.* **2022**, *349*, No. 131441. Gao, S.; Peng, H.; Song, B.; Zhang, J.; Wu, W.; Vaughan, J.; Zardo, P.; Vogrin, J.; Tulloch, S.; Zhu, Z. Synthesis of zeolites from low-cost feeds and its sustainable environmental applications. *J. Environ. Chem. Eng.* **2023**, *11* (1), No. 108995.

(15) Tao, Z.; Tian, Y.; Hanif, A.; Chan, V.; Gu, Q.; Shang, J. Metal cation-exchanged LTA zeolites for CO2/N2 and CO2/CH4 separation: The roles of gas-framework and gas-cation interactions. *Carbon Capture Sci. Technol.* **2023**, *8*, No. 100126.

(16) Wang, Y.; Jia, H.; Chen, P.; Fang, X.; Du, T. Synthesis of La and Ce modified X zeolite from rice husk ash for carbon dioxide capture. *J. Mater. Res. Technol.* **2020**, *9* (3), 4368−4378.

(17) Liu, Q.; Mace, A.; Bacsik, Z.; Sun, J.; Laaksonen, A.; Hedin, N. NaKA sorbents with high CO2-over-N2 selectivity and high capacity to adsorb CO2. *Chem. Commun.* **2010**, *46* (25), 4502−4504.

(18) Wang, Y.; Du, T.; Jia, H.; Qiu, Z.; Song, Y. Effect of extra-framework cation in ion-exchanged ZSM-5 from rice husk ash on CO2 adsorption. *Solid State Sci.* **2019**, *97*, No. 105985.

(19) Yang, R. T. *Zeolites and Molecular Sieves*; John Wiley & Sons, Inc., 2003 DOI: 10.1002/047144409X.ch7.

(20) Yang, R. T. Zeolites and Molecular Sieves. In *Adsorbents: Fundamentals and Applications*; Wiley, 2003; pp 157−190.

(21) Ke, G.; Shen, H.; Yang, P. Synthesis of X-Zeolite from Waste Basalt Powder and its Influencing Factors and Synthesis Mechanism. *Materials* **2019**, *12*, 3895.

(22) Tobarameekul, P.; Sangsuradet, S.; Worathanakul, P. Comparative Study of Zn Loading on Advanced Functional Zeolite NaY from Bagasse Ash and Rice Husk Ash for Sustainable CO2 Adsorption with ANOVA and Factorial Design. *Atmosphere* **2022**, *13* (2), 314.

(23) Pal, N.; Pramanik, M.; Bhaumik, A.; Ali, M. Highly selective and direct oxidation of cyclohexane to cyclohexanone over vanadium exchanged NaY at room temperature under solvent-free conditions. *J. Mol. Catal. A: Chem.* **2014**, *392*, 299−307.

(24) Cheung, O.; Bacsik, Z.; Liu, Q.; Mace, A.; Hedin, N. Adsorption kinetics for CO2 on highly selective zeolites NaKA and nano-NaKA. *Appl. Energy* **2013**, *112*, 1326−1336.

(25) Mokrzycki, J.; Fedyna, M.; Marzec, M.; Szerement, J.; Panek, R.; Klimek, A.; Bajda, T.; Mierzwa-Hersztek, M. Copper ion-exchanged zeolite X from fly ash as an efficient adsorbent of phosphate ions from aqueous solutions. *J. Environ. Chem. Eng.* **2022**, *10* (6), No. 108567.

(26) Han, J.; Liu, C.; Liu, Q.; Lu, S.; Bi, Y.; Wang, X.; Guo, M.; Song, C.; Ji, N.; Lu, X.; et al. Cu-exchanged Al-rich OFF-CHA twin-crystal zeolite for the selective catalytic reduction of NOx by NH3. *Catal. Today* **2021**, *376*, 87−94.

(27) Yao, G.; Lei, J.; Zhang, W.; Yu, C.; Sun, Z.; Zheng, S.; Komarneni, S. Antimicrobial activity of X zeolite exchanged with Cu2+ and Zn2+ on *Escherichia coli* and Staphylococcus aureus. *Environ. Sci. Pollut. Res.* **2019**, *26* (3), 2782−2793.

(28) Benaliouche, F.; Boucheffa, Y.; Ayrault, P.; Mignard, S.; Magnoux, P. NH3-TPD and FTIR spectroscopy of pyridine adsorption studies for characterization of Ag- and Cu-exchanged X zeolites. *Microporous Mesoporous Mater.* **2008**, *111* (1), 80−88.

(29) Zhukov, Y. M.; Shelyapina, M. G.; Zvereva, I. A.; Efimov, A. Y.; Petranovskii, V. Microwave assisted versus convention Cu2+ exchange in mordenite. *Microporous Mesoporous Mater.* **2018**, *259*, 220−228.

(30) Hassan, H.; Hameed, B. H. Oxidative decolorization of Acid Red 1 solutions by Fe−zeolite Y type catalyst. *Desalination* **2011**, *276* (1), 45−52.

(31) Murukutti, M. K.; Jena, H. Synthesis of nano-crystalline zeolite-A and zeolite-X from Indian coal fly ash, its characterization and performance evaluation for the removal of Cs+ and Sr2+ from simulated nuclear waste. *J. Hazard. Mater.* **2022**, *423*, No. 127085.

(32) Wang, P.; Sun, Q.; Zhang, Y.; Cao, J.; Li, X. Hydrothermal synthesis of Zeolite NaA from Kaolin. *Funct. Mater. Lett.* **2019**, *12* (05), No. 1950075.

(33) Muriithi, G. N.; Petrik, L. F.; Doucet, F. J. Synthesis, characterisation and CO2 adsorption potential of NaA and NaX zeolites and hydrotalcite obtained from the same coal fly ash. *J. CO2 Util.* **2020**, *36*, 220−230.

(34) Price, L.; Leung, K. M.; Sartbaeva, A. Local and Average Structural Changes in Zeolite A upon Ion Exchange. *Magnetochemistry* **2017**, *3*, 42.

(35) Wang, P.; Cao, J.; Zhang, Y.; Sun, Q. Controllable Preparation of Cubic Zeolite A and Application of Langmuir Model in Carbon Dioxide Adsorption. *Nanomaterials* **2021**, *11*, 3375.

(36) Djamel, N.; Samira, A. Mechanism of Cu2+ ions uptake process by synthetic NaA zeolite from aqueous solution: Characterization,

https://doi.org/10.1021/acsomega.4c05487
ACS Omega 2024, 9, 45926−45942

Kinetic, intra-crystalline diffusion and thermodynamic studies. *J. Mol. Liq.* **2021**, *323*, No. 114642.
(37) Alswat, A. A.; Ahmad, M. B.; Hussein, M. Z.; Ibrahim, N. A.; Saleh, T. A. Copper oxide nanoparticles-loaded zeolite and its characteristics and antibacterial activities. *J. Mater. Sci. Technol.* **2017**, *33* (8), 889−896.
(38) Mohamed, E. F.; Awad, G.; Zaitan, H.; Andriantsiferana, C.; Manero, M. H. Transition metals-incorporated zeolites as environmental catalysts for indoor air ozone decomposition. *Environ. Technol.* **2018**, *39* (7), 878−886.
(39) Nezamzadeh-Ejhieh, A.; Hushmandrad, S. Solar photodecolorization of methylene blue by CuO/X zeolite as a heterogeneous catalyst. *Appl. Catal., A* **2010**, *388* (1), 149−159.
(40) Pereira, P. M.; Ferreira, B. F.; Oliveira, N. P.; Nassar, E. J.; Ciuffi, K. J.; Vicente, M. A.; Trujillano, R.; Rives, V.; Gil, A.; Korili, S.; De Faria, E. Synthesis of Zeolite A from Metakaolin and Its Application in the Adsorption of Cationic Dyes. *Appl. Sci.* **2018**, *8* (4), 608.
(41) Ayele, L.; Pérez-Pariente, J.; Chebude, Y.; Diaz, I. Synthesis of zeolite A using kaolin from Ethiopia and its application in detergents. *New J. Chem.* **2016**, *40* (4), 3440−3446.
(42) Nadeem, S.; Mutalib, I. A.; Shahrun, M. S. Synthesis of Metalloporphyrin Encapsulated Zeolite A for Photocatalytic Orange II Degradation. *Procedia Eng.* **2016**, *148*, 1282−1288.
(43) Khoramzadeh, E.; Mofarahi, M.; Lee, C.-H. Equilibrium Adsorption Study of CO2 and N2 on Synthesized Zeolites 13X, 4A, 5A, and Beta. *J. Chem. Eng. Data* **2019**, *64* (12), 5648−5664.
(44) Wang, P.; Sun, Q.; Zhang, Y.; Cao, J. Synthesis of Zeolite 4A from Kaolin and Its Adsorption Equilibrium of Carbon Dioxide. *Materials* **2019**, *12* (9), 1536.
(45) Shi, H.; Zhang, J.; Li, J. The effect of guest cations on proton conduction of LTA zeolite. *RSC Adv.* **2021**, *11* (10), 5393−5398. Cui, J.; Yeasmin, R.; Shao, Y.; Zhang, H.; Zhang, H.; Zhu, J. Fabrication of Ag+, Cu2+, and Zn2+ Ternary Ion-Exchanged Zeolite as an Antimicrobial Agent in Powder Coating. *Ind. Eng. Chem. Res.* **2020**, *59* (2), 751−762.
(46) Yao, G.; Lei, J.; Zhang, X.; Sun, Z.; Zheng, S. One-Step Hydrothermal Synthesis of Zeolite X Powder from Natural Low-Grade Diatomite. *Materials* **2018**, *11* (6), 906.
(47) Goldstein, J. I.; Newbury, D. E.; Echlin, P.; Joy, D. C.; Lyman, C. E.; Lifshin, E.; Sawyer, L.; Michael, J. R. X-Ray Spectral Measurement: EDS and WDS. In *Scanning Electron Microscopy and X-ray Microanalysis*, Third ed.; Goldstein, J. I.; Newbury, D. E.; Echlin, P.; Joy, D. C.; Lyman, C. E.; Lifshin, E.; Sawyer, L.; Michael, J. R., Eds.; Springer US, 2003; pp 297−353.
(48) Williams, D. B.; Carter, C. B. Quantitative X-ray Analysis. In *Transmission Electron Microscopy: A Textbook for Materials Science*; Williams, D. B.; Carter, C. B., Eds.; Springer US, 2009; pp 639−662.
(49) Guisnet, M.; Gilson, J. P. INTRODUCTION TO ZEOLITE SCIENCE AND TECHNOLOGY. In *Zeolites for Cleaner Technologies*, Catalytic Science Series; PUBLISHED BY IMPERIAL COLLEGE PRESS AND DISTRIBUTED BY WORLD SCIENTIFIC PUBLISHING CO., 2002; Vol. 3, pp 1−28.
(50) Larin, A. V. The Loewenstein rule: the increase in electron kinetic energy as the reason for instability of Al−O−Al linkage in aluminosilicate zeolites. *Phys. Chem. Miner.* **2013**, *40* (10), 771−780.
(51) Tahraoui, Z.; Nouali, H.; Marichal, C.; Forler, P.; Klein, J.; Daou, T. J. Influence of the Compensating Cation Nature on the Water Adsorption Properties of Zeolites. *Molecules* **2020**, *25* (4), 944.
(52) Bardestani, R.; Patience, G. S.; Kaliaguine, S. Experimental methods in chemical engineering: specific surface area and pore size distribution measurements—BET, BJH, and DFT. *Can. J. Chem. Eng.* **2019**, *97* (11), 2781−2791.
(53) Jasra, R. V.; Choudary, N. V.; Bhat, S. G. T. Correlation of Sorption Behavior of Nitrogen, Oxygen, and Argon with Cation Locations in Zeolite X. *Ind. Eng. Chem. Res.* **1996**, *35* (11), 4221−4229.
(54) Rakoczy, R. A.; Traa, Y. Nanocrystalline zeolite A: synthesis, ion exchange and dealumination. *Microporous Mesoporous Mater.* **2003**, *60* (1), 69−78.
(55) Tian, J.; Peng, H.; Xu, X.; Liu, W.; Ma, Y.; Wang, X.; Yang, X. High surface area La2Sn2O7 pyrochlore as a novel, active and stable support for Pd for CO oxidation. *Catal. Sci. Technol.* **2015**, *5* (4), 2270−2281.
(56) Gligor, D.; Maicaneanu, S. A.; Varodi, C. Low-Cost Carbon Paste Cu(II)-Exchanged Zeolite Amperometric Sensor for Hydrogen Peroxide Detection. *Chemosensors* **2024**, *12* (2), 23.
(57) Gatta, G. D.; Cappelletti, P.; de' Gennaro, B.; Rotiroti, N.; Langella, A. New data on Cu-exchanged phillipsite: a multi-methodological study. *Phys. Chem. Miner.* **2015**, *42* (9), 723−733.
(58) Zhang, M.; Wang, X. Preparation of a Gangue-Based X-type Zeolite Molecular Sieve as a Multiphase Fenton Catalyst and Its Catalytic Performance. *ACS Omega* **2021**, *6* (28), 18414−18425.
(59) Arcibar-Orozco, J. A.; Flores-Rojas, A. I.; Rangel-Mendez, J. R.; Díaz-Flores, P. E. Synergistic effect of zeolite/chitosan in the removal of fluoride from aqueous solution. *Environ. Technol.* **2020**, *41* (12), 1554−1567.
(60) Langmi, H. W.; Book, D.; Walton, A.; Johnson, S. R.; Al-Mamouri, M. M.; Speight, J. D.; Edwards, P. P.; Harris, I. R.; Anderson, P. A. Hydrogen storage in ion-exchanged zeolites. *J. Alloys Compd.* **2005**, *404*−*406*, 637−642.
(61) Pham, T. D.; Liu, Q.; Lobo, R. F. Carbon Dioxide and Nitrogen Adsorption on Cation-Exchanged SSZ-13 Zeolites. *Langmuir* **2013**, *29* (2), 832−839.
(62) Zhang, C.; Zhang, D.; Zhang, X.; Chen, X.; Chen, L.; Tian, Y.; Wang, L. Rubik's cube-shaped Linde type A zeolite synthesized from biomass for carbon dioxide capture. *Cell Rep. Phys. Sci.* **2024**, *5* (4), No. 101889.
(63) Zhang, P.; Li, S.; Zhang, C. Solvent-free synthesis of nano-cancrinite from rice husk ash. *Biomass Convers. Biorefin.* **2019**, *9* (3), 641−649.
(64) Silva, D. P. S.; Santos, A. T.; Ribeiro, T. R. S.; Solano, J. R. S.; Cavalcanti, R. K. B. C.; Silva, B. J. B.; Quintela, P. H. L.; Silva, A. O. S. Monosodium glutamate-mediated hierarchical porous formation in LTA zeolite to enhance CO2 adsorption performance. *J. Sol−Gel Sci. Technol.* **2021**, *100* (2), 360−372.
(65) Czuma, N.; Casanova, I.; Baran, P.; Szczurowski, J.; Zarębska, K. CO2 sorption and regeneration properties of fly ash zeolites synthesized with the use of differentiated methods. *Sci. Rep.* **2020**, *10* (1), No. 1825.
(66) Schwanke, A. J.; Balzer, R.; Pergher, S. Microporous and Mesoporous Materials from Natural and Inexpensive Sources. In *Handbook of Ecomaterials*; Martínez, L. M. T.; Kharissova, O. V.; Kharisov, B. I., Eds.; Springer International Publishing, 2017; pp 1−22.
(67) Salehi, S.; Anbia, M. Characterization of CPs/Ca-exchanged FAU- and LTA-type zeolite nanocomposites and their selectivity for CO2 and N2 adsorption. *J. Phys. Chem. Solids* **2017**, *110*, 116−128.
(68) Jia, H.; Du, T.; Fang, X.; Gong, H.; Qiu, Z.; Li, Y.; Wang, Y. Synthesis of Template-Free ZSM-5 from Rice Husk Ash at Low Temperatures and Its CO2 Adsorption Performance. *ACS Omega* **2021**, *6* (5), 3961−3972.
(69) Bae, T.-H.; Hudson, M. R.; Mason, J. A.; Queen, W. L.; Dutton, J. J.; Sumida, K.; Micklash, K. J.; Kaye, S. S.; Brown, C. M.; Long, J. R. Evaluation of cation-exchanged zeolite adsorbents for post-combustion carbon dioxide capture. *Energy Environ. Sci.* **2013**, *6* (1), 128−138.
(70) Boer, D. G.; Langerak, J.; Pescarmona, P. P. Zeolites as Selective Adsorbents for CO2 Separation. *ACS Appl. Energy Mater.* **2023**, *6* (5), 2634−2656.
(71) Maesen, T.; Marcus, B. Chapter 1 The zeolite scene—An overview. In *Studies in Surface Science and Catalysis*; van Bekkum, H.; Flanigen, E. M.; Jacobs, P. A.; Jansen, J. C., Eds.; Elsevier, 2001; Vol. *137*, pp 1−9.
(72) Boer, D. G.; Langerak, J.; Pescarmona, P. P. Zeolites as Selective Adsorbents for CO2 Separation. *ACS Appl. Energy Mater.* **2023**, *6*, 2634.
(73) Zukal, A.; Arean, C. O.; Delgado, M. R.; Nachtigall, P.; Pulido, A.; Mayerová, J.; Čejka, J. Combined volumetric, infrared spectroscopic and theoretical investigation of CO2 adsorption on Na-A zeolite. *Microporous Mesoporous Mater.* **2011**, *146* (1), 97−105. Cheung, O.;

https://doi.org/10.1021/acsomega.4c05487
ACS Omega 2024, 9, 45926−45942

Wardecki, D.; Bacsik, Z.; Vasiliev, P.; McCusker, L. B.; Hedin, N. Highly selective uptake of carbon dioxide on the zeolite | Na10.2KCs0.8|-LTA − a possible sorbent for biogas upgrading. *Phys. Chem. Chem. Phys.* **2016**, *18* (24), 16080−16083.
(74) Calleja, G.; Pau, J.; Calles, J. A. Pure and Multicomponent Adsorption Equilibrium of Carbon Dioxide, Ethylene, and Propane on ZSM-5 Zeolites with Different Si/Al Ratios. *J. Chem. Eng. Data* **1998**, *43* (6), 994−1003. Chen, H.; Wang, W.; Ding, J.; Wei, X.; Lu, J. CO2 Adsorption Capacity of FAU Zeolites in Presence of H2O: A Monte Carlo Simulation Study. *Energy Procedia* **2017**, *105*, 4370−4376.
(75) Krachuamram, S.; Chanapattharapol, K. C.; Kamonsutthipaijit, N. Synthesis and characterization of NaX-type zeolites prepared by different silica and alumina sources and their CO2 adsorption properties. *Microporous Mesoporous Mater.* **2021**, *310*, No. 110632.
(76) Abunowara, M.; Bustam, M. A.; Sufian, S.; Eldemerdash, U. Description of Carbon Dioxide Adsorption and Desorption onto Malaysian Coals under Subcritical Condition. *Procedia Eng.* **2016**, *148*, 600−608.
(77) Siriwardane, R. V.; Shen, M.-S.; Fisher, E. P. Adsorption of CO2, N2, and O2 on Natural Zeolites. *Energy Fuels* **2003**, *17* (3), 571−576.
(78) Espinal, L.; Wong-Ng, W.; Kaduk, J. A.; Allen, A. J.; Snyder, C. R.; Chiu, C.; Siderius, D. W.; Li, L.; Cockayne, E.; Espinal, A. E.; Suib, S. L. Time-Dependent CO2 Sorption Hysteresis in a One-Dimensional Microporous Octahedral Molecular Sieve. *J. Am. Chem. Soc.* **2012**, *134* (18), 7944−7951.
(79) de Oliveira, L. H.; Pereira, M. V.; Meneguin, J. G.; de Barros, M. A. S. D.; do Nascimento, J. F.; Arroyo, P. A. Influence of regeneration conditions on cyclic CO2 adsorption on NaA zeolite at high pressures. *J. CO2 Util.* **2023**, *67*, No. 102296.
(80) Breck, D. W. Zeolite molecular sieves: structure, chemistry, and use. *Anal. Chim. Acta* **1974**, *75* (2), 493.
(81) Giannetto Pace, G. *Zeolitas: características, propiedades y aplicaciones industriales; Ed.ial Innovación Tecnológica*; Facultad de Ingeniería, UCV, 2000.
(82) Gunawan, T.; Wijiyanti, R.; Widiastuti, N. Adsorption−desorption of CO2 on zeolite-Y-templated carbon at various temperatures. *RSC Adv.* **2018**, *8* (72), 41594−41602. 10.1039/C8RA09200A. Mukhtar, A.; Mellon, N.; Saqib, S.; Lee, S.-P.; Bustam, M. A. Extension of BET theory to CO2 adsorption isotherms for ultra-microporosity of covalent organic polymers. *SN Appl. Sci.* **2020**, *2* (7), No. 1232.
(83) Panda, D.; Kumar, E. A.; Singh, S. K. Amine Modification of Binder-Containing Zeolite 4A Bodies for Post-Combustion CO2 Capture. *Ind. Eng. Chem. Res.* **2019**, *58* (13), 5301−5313.
(84) Coluccia, S.; Marchese, L.; Martra, G. Characterisation of microporous and mesoporous materials by the adsorption of molecular probes: FTIR and UV−Vis studies. *Microporous Mesoporous Mater.* **1999**, *30* (1), 43−56.
(85) Liu, Q.; Jiang, J.; Zhang, F.; Jia, X.; Cheng, H.; Krasilin, A.; Ouyang, J. CO2 fixation mechanism of kaolin treated with organic amines at varied temperatures and pressure. *Appl. Clay Sci.* **2022**, *228*, No. 106638.
(86) Yi, H.; Deng, H.; Tang, X.; Yu, Q.; Zhou, X.; Liu, H. Adsorption equilibrium and kinetics for SO2, NO, CO2 on zeolites FAU and LTA. *J. Hazard. Mater.* **2012**, *203*−*204*, 111−117.
(87) Shang, J.; Li, G.; Singh, R.; Gu, Q.; Nairn, K. M.; Bastow, T. J.; Medhekar, N.; Doherty, C. M.; Hill, A. J.; Liu, J. Z.; Webley, P. A. Discriminative Separation of Gases by a "Molecular Trapdoor" Mechanism in Chabazite Zeolites. *J. Am. Chem. Soc.* **2012**, *134* (46), 19246−19253.
(88) Lozinska, M. M.; Mowat, J. P. S.; Wright, P. A.; Thompson, S. P.; Jorda, J. L.; Palomino, M.; Valencia, S.; Rey, F. Cation Gating and Relocation during the Highly Selective "Trapdoor" Adsorption of CO2 on Univalent Cation Forms of Zeolite Rho. *Chem. Mater.* **2014**, *26* (6), 2052−2061.
(89) Thakkar, H.; Issa, A.; Rownaghi, A. A.; Rezaei, F. CO2 Capture from Air Using Amine-Functionalized Kaolin-Based Zeolites. *Chem. Eng. Technol.* **2017**, *40* (11), 1999−2007.
(90) Tao, Z.; Tian, Y.; Ou, S. Y.; Gu, Q.; Shang, J. Direct air capture of CO2 by metal cation-exchanged LTA zeolites: Effect of the charge-to-size ratio of cations. *AIChE J.* **2023**, *69* (8), No. e18139.
(91) Najafi, A. M.; Soltanali, S.; Ghassabzadeh, H. Enhancing the CO2, CH4, and N2 adsorption and kinetic performance on FAU zeolites for CO2 capture from flue gas by metal incorporation technique. *Chem. Eng. J.* **2023**, *468*, No. 143719.
(92) Lee, K.-M.; Lim, Y.-H.; Park, C.-J.; Jo, Y.-M. Adsorption of Low-Level CO2 Using Modified Zeolites and Activated Carbon. *Ind. Eng. Chem. Res.* **2012**, *51* (3), 1355−1363.
(93) Ahmad, K.; Mowla, O.; Kennedy, E. M.; Dlugogorski, B. Z.; Mackie, J. C.; Stockenhuber, M. A Melamine-Modified β-Zeolite with Enhanced CO2 Capture Properties. *Energy Technol.* **2013**, *1* (5−6), 345−349.

https://doi.org/10.1021/acsomega.4c05487
ACS Omega 2024, 9, 45926−45942